Heat transport modeling in shallow aquifers

The role of thermal dispersion in aquifers and heat conduction into confining layers

Dissertation

der Mathematisch-Naturwissenschaftlichen Fakultät
der Eberhard Karls Universität Tübingen
zur Erlangung des Grades eines Doktors der Naturwissenschaften
(Dr. rer. nat.)

vorgelegt von
Nelson Molina-Giraldo
aus Medellín, Kolumbien

Tübingen

2011

Tag der mündlichen Qualifikation:	22.07.2011
Dekan:	Prof. Dr. Wolfgang Rosenstiel
1. Berichterstatter:	Jun.-Prof. Dr. habil. Philipp Blum
2. Berichterstatter:	Prof. Dr.-Ing. Olaf A. Cirpka

Acknowledgments

First of all, I would like to thank my supervisors Dr. Peter Bayer, Jun.-Prof. Philipp Blum and Prof. Olaf A. Cirpka for their valuable help and for giving me the opportunity to become active part of the ZAG group. I am also very thankful to Prof. Peter Grathwohl for the fruitful discussions we had about heat transport. I also want to thank the program IPSWaT (International Postgraduate Studies in Water Technologies) for economical support during my PhD, as well as my colleagues Jozsef Hecht Mendez, Anibal Perez Garcia, Stefanie Hähnlein, Ke Zhu and Fernando Mazo D'Affonseca for being so helpful whenever I needed them. The support of Margaret Hass in preparing the manuscripts is also gratefully acknowledged. I also acknowledge Prof. Fang from Shandong Jianzhu University for the successful mutual collaboration. I am also thankful to Dr. Peter Merkel and Monika Jekelius for their support regarding administrative matters. Finally, thanks to my family and my wife for their unconditional support during this adventure in Germany.

Abstract

Heat transfer by conduction through the fluid and solid phase and advection through the moving water mainly determine the heat transport in the subsurface. Additionally, heat transfer by thermal dispersion occurs due to differential advection at the pore-scale and heterogeneities of the permeability field at macroscopic scales. Compare to solute diffusion coefficients, heat diffusion coefficients are normally higher. This difference has led to dissimilar ways of treating the processes and the boundary conditions in heat and contaminant transport simulations. In particular, effects of hydrodynamic dispersion in aquifers and diffusion through the confining layers. Most conceptualizations of heat transport in the underground neglect these processes and the error introduced is not often evaluated. Hence, in the present study, an analytical and numerical modeling study is carried out to evaluate the effect of such simplifications on heat transport simulations.

Two practical applications of heat transport in the subsurface are used to tackle these problems: Low-enthalpy geothermal systems and natural temperature variations as hydrogeological tracer. A concise discussion of the effect of thermal dispersion on the simulation of temperature plumes in aquifers that evolve from vertical ground source heat pump systems is presented. Results indicate that the effect of thermal dispersion on the temperature plume distribution around a borehole heat exchanger can be neglected if thermal dispersion depends only on the Peclet number. On the other hand, thermal dispersion has a larger effect on temperature plume distribution when thermal dispersivity is assumed to be scale-dependent for aquifers where medium sands and gravel dominate.

In order to evaluate the effects of conduction into confining layers, an analytical solution which considers groundwater flow and axial effects is developed. Comparison with existing analytical solutions which either neglect groundwater velocity or axial effects shows the importance of these two processes when evaluating the temperature response of a borehole heat exchanger. In general, for moderate groundwater flow scenarios, the combined effect of advection and axial effects must be accounted for. The importance of axial effects is also corroborated by analyzing the heat transport process by using heat as a tracer. Comparison of different conceptual simplifications of an infiltrating

river carrying a temperature signal into an adjacent aquifer is carried out. Results show that temperature propagation within the aquifer can by highly influenced by conduction through the unsaturated zone and the underlying aquitard. The analytical and numerical modeling approaches presented in the present PhD thesis contribute to advance in the understanding of heat transport in the subsurface, mainly in the regulation, monitoring and design of low-enthalpy geothermal systems and hydrogeological interpretations by means of temperature signals.

Einleitung

Im Untergrund wird Wärme in der Flüssig– und Festphase hauptsächlich durch Konduktion und im bewegten Fluid durch Advektion transportiert. Als thermische Dispersion bezeichnet man den Effekt der differentiellen Advektion, die sich aus unterschiedlichen Geschwindigkeiten auf der Porenskala und Heterogenitäten der Permeabilität im makroskopischen Raum ergibt. Im Vergleich zu Schadstoffdiffusionskoeffizienten sind Wärmediffusionskoeffizienten gewöhnlich größer. Dieser Unterschied führt zu einer unterschiedlichen Betrachtung der Prozesse und der Randbedingungen in Wärme- und Schadstofftransportsimulationen. Besonders die Auswirkungen von hydrodynamischer Dispersion in Aquiferen und Diffusion in begrenzende Schichten von geringer Permeabilität. Aus diesem Grund berücksichtigen die meisten Konzepte zur Beschreibung des Wärmetransportes im Untergrund die thermische Dispersion in Aquiferen und die Konduktion in angrenzende Schichten nicht. Entsprechend wird der Fehler, der durch diese Vereinfachung entsteht, vernachlässigt. In der vorliegenden Dissertation wird anhand von analytischen und numerischen Modellen der Effekt der thermischen Diffusion in angrenzende Schichten und die Rolle der thermischen Dispersion bei der Simulation von Wärmetransport erörtert. Hierzu werden zwei praktische Anwendungen des Wärmetransportes im Untergrund herangezogen: Flache Geothermie und natürliche Temperaturschwankungen als Tracer. Der Einfluss der thermischer Dispersion in Simulationen von Temperaturanomalien bei der Nutzung von vertikalen Erdwärmesonden wird umfassend beschrieben. Die Ergebnisse zeigen das der Einfluss der thermischer Dispersion auf die Verteilung der Temperaturfahne von vertikalen Erdwärmesonden vernachlässigbar ist, wenn diese ausschließlich von der Pecletzahl abhängt oder der Aquifer homogen ist. Dagegen hat die thermische Dispersion auf Temperaturanomalien in heterogenen Aquiferen größeren Einfluss, wenn die Korngrößen von Mittelsand bis Kies dominieren und die thermische Dispersivität maßstabsabhängig ist. Um die Auswirkungen der Konduktion auf angrenzende Schichten zu analysieren, wurde eine analytische Gleichung entwickelt, die den Grundwasserfluß und die axialen Effekte berücksichtigt. Vergleiche mit bestehenden analytischen Gleichungen, die entweder die Grundwasserfließgeschwindigkeit oder den axialen Effekt vernachlässigen, zeigen die Wichtigkeit der Kombination dieser Aspekte für die Analyse

der Temperaturveränderungen von Erdwärmesonden. Grundsätzlich müssen für moderate Grundwasserszenarien Advektion und axial Effekte im Zusammenspiel berücksichtigt werden. Die Bedeutung des Axialeffekts tritt auch bei der Analyse der Wärmetransportprozesse mit Wärme als Tracer in den Vordergrund. Verschiedene konzeptionelle Modelle eines infiltrierenden Flusses mit Temperatursignalen in einen angrenzenden Aquifer wurden verglichen. Diese Ergebnisse zeigen, dass die Veränderung des Temperatursignals im Aquifer von der Konduktion sowohl durch den unterlagernden Aquitard als auch durch die ungesättigte Zone beeinflusst wird. Die analytischen und numerischen Modelle der vorliegenden Studie ermöglichen ein umfassendes und erweitertes Prozessverständnis von Wärmetransport im Untergrund, hinsichtlich der Steuerung, dem Monitoring und Design von flachen geothermischen Systemen zur effizienten Nutzung von Erdwärme, sowie der hydrogeologischen Interpretation mittels saisonalen Temperatursignalen.

Contents

Nomenclature

a	thermal diffusivity [m^2/s]
a_T	temperature amplitude [K]
c	specific heat capacity [J/kg/K]
c_{wave}	celerity of the sinusoidal wave propagation [m/s]
d	mean particle diameter [m]
D	dispersion tensor [m^2/s]
f	frequency [1/s]
Fo	Fourier number [-]
h	hydraulic head [m]
h_c	capillary head [m]
H	borehole heat exchanger length [m]
k	complex decay coefficient [1/m]
K	hydraulic conductivity [m/s]
K_0	modified Bessel function of second kind and order zero
L	field scale [m]
L_p	length of temperature plume [m]
Pe	Peclet number [-]
q	Darcy velocity [m/s]
Q	heat flow rate extraction or injection [J/s]
Q'	energy extracted or injected [J]
q_L	heat flow rate per unit length of the borehole [W/m]
r	radial distance to the source [m]
r'	radial coordinate [m]
R_T	retardation factor [-]
R, R', Z, Z'	dimensionless coordinates [-]
s	volumetric heat source [W/m^3]
S_e	effective water saturation [-]
t	time [s]
T	average temperature of the porous medium [°C]
T_o	undisturbed initial temperature of the porous medium [°C]
ΔT	temperature change (T_o-T) [°C]
v_a	seepage velocity [m/s]
v_T	effective heat transport velocity [m/s]
u	integration parameter
x_p	penetration depth [m]

x, y, z	space coordinates [m]
Greek symbols	
α, N	van-Genuchten parameters. [1/m] and [-] respectively
α_x	longitudinal thermal dispersivity [m]
α_y	transverse thermal dispersivity [m]
λ	thermal conductivity [W/m/K]
λ_x	effective longitudinal thermal conductivity [W/m/K]
λ_y	effective transverse thermal conductivity [W/m/K]
ρ	density [kg/m^3]
φ	polar angle [-]
ϕ	phase shift [-]
ψ	integration parameters
θ	Porosity [-]
Θ	dimensionless temperature
Θ_w	volumetric water content [-]
Subscripts	
g	gas phase
m	porous medium, mean temperature around a circle
s	aquifer material (solids), steady-state
w	water phase

1. Introduction

1.1. Background and objectives

Heat transport theories are already well established and have been studied for several decades (Carslaw and Jaeger 1959). However, attention on heat transport simulation in the underground has been continuously increasing in the last years in areas such as heat as a tracer (Anderson 2005), geothermal energy (Ferguson 2009), and variable-density flow (Ma and Zheng 2010). Heat transport in the subsurface can be described mainly by conduction through the solid phase, and heat exchange between the solid and fluid phase. For most practical applications, local thermal equilibrium is assume and the temperature of the solid and fluid phase are usually taken to be the same (de Marsily 1986; Moyne et al. 2000). Additionally, heat transfer by advection through the moving water is accomplished when groundwater flow is present in the subsurface. Differential groundwater flow paths at the pore-scale and heterogeneity of the permeability field at macroscopic scales create the so-called thermal dispersion.

Transfer of heat due to thermal gradients is much more efficient than transfer of solute due to gradients of concentration. Hence, heat diffusion coefficients are normally higher than solute diffusion coefficients, with differences up to two orders of magnitude (Bear 1972; Domenico and Schwartz 1998). This difference has lead to dissimilar ways of conceptualizing the processes and the boundary conditions in heat and contaminant transport simulations. Thermal dispersion, for instance, has usually been neglected in heat transport problems (Bear 1972; Woodbury and Smith 1985) because of the dominance of thermal diffusion. However, heat transport in the subsurface might be affected by mechanical mixing depending on the nature of the aquifer (Ferguson 2007; Hidalgo et al. 2009; Nield and Bejan 2006). Regarding boundary conditions, unlike in contaminant transport, in heat transport simulations the effect of considering confining layers on the overall transport process in the aquifer might be of higher interest. Confining layers act as a sink and source of heat and axial effects may play an important role due to the high thermal diffusion coefficients.

In order to address the aforementioned problems, two practical application of heat transport in the subsurface are used: natural temperature variation as hydrogeological tracer and low-enthalpy geothermal energy. The former refers to the used of temporal fluctuation of temperature for hydrogeological interpretation. Heat as a tracer can be used, for instance, to evaluate groundwater-surface water interaction and to determine hydraulic parameters of the underground by coupling groundwater flow and heat transport models (Anderson 2005). Low-enthalpy geothermal energy refers to the use of heat stored in the shallow underground (< 400 m) and in aquifers, mainly by ground source heat pump (GSHP) systems, which can be employed as heating/cooling devices to supply buildings of any size (Lund et al. 2005).

In particular I want to answer the following research questions:

- Thermal dispersion is often neglected in heat transport problems. However, for the regulation and monitoring of low-enthalpy geothermal systems, what is the effect of neglecting it when simulating temperature plume distributions around a BHE under typical hydrogeological conditions?
- Analytical solutions to estimate the heat transfer at the GSHP systems usually neglect either groundwater flow or axial effects. Under which operational conditions and groundwater flow scenarios become the axial effects important?
- Travel times of temperature signals at infiltration wells are usually interpreted with over simplistic numerical and analytical methods. What is influence of conceptual simplifications such as conduction into the aquitard and top layer on the accuracy of the simulations of the temperature distribution in the aquifer?

1.2. Thesis outline

The structure of the thesis is as follows: Chapter 2 consists of a general overview of the use of heat as a tracer and low-enthalpy geothermal energy. In Chapter 3, 4, the influence of axial effects on heat transport simulations is addressed. Propagation of seasonal temperature fluctuations into an aquifer (Chapter 3) is used as a practical application to evaluate the effect of over-simplification of boundary conditions in heat transport problems. Chapter 4 describes a new analytical approach which is proposed to evaluate axial effects on the heat transfer in shallow geothermal systems. In Chapter 5 the effect of

neglecting thermal dispersion on temperature plumes from geothermal system is addressed. Finally, a summary and general conclusion of Chapters 3, 4 and 5 are presented.

2. General overview

2.1. Low-enthalpy shallow geothermal energy

During the last two decades, the usage of geothermal energy has shown a recurrent increase in most countries of the world, often with exponential growth rates of capacity and of the number of installations (Lund et al. 2010). High-enthalpy systems utilize geothermal resources with high thermodynamic energy and are commonly applied for power generation. On the other hand, low-enthalpy geothermal systems have a huge potential, even beyond their traditional application for recreation and medicinal purposes (Clauser 2006).

These generally use the heat available in the shallow subsurface (< 400 m), and can be employed to provide heating and cooling to buildings of any size. Among these shallow geothermal systems, vertical ground source heat pump (GSHP) systems are one of the major technologies for heating/cooling purposes in many countries (Hähnlein et al. 2010b). GSHP are closed systems which consist of an aboveground heat pump (HP) and a borehole heat exchanger (BHE) (Figure 2-1). Heat exchange between the underground and the heat pump is accomplished by circulating a heat carrier fluid within the pipes of the BHE which is usually installed up to depths of around 150 m (Mustafa Omer 2008).

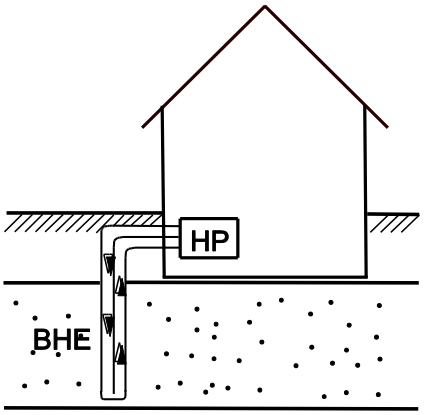

Figure 2-1. Ground source heat pump (GSHP) system.

Vertical heat transfer at the BHE can be estimated by different analytical approaches (Bandos et al. 2009; Carslaw and Jaeger 1959; Diao et al. 2004; Eskilson 1987; Man et al. 2010; Michopoulos and Kyriakis 2009; Sutton et al. 2003; Yang et al. 2009; Zeng et al. 2002; Ingersoll et al. 1954; Hähnlein et al. 2010a). Pioneer work was made by Ingersoll et al. (1954) who applied analytical solutions given by Carslaw and Jaeger (1959) such as the infinite line source model (ILS) and infinite cylindrical source model (ICS) to BHE. The ILS and ICS consider the BHE as an infinite line (or cylindrical) source along the vertical direction and are not suitable for long time simulation due to the fact that they cannot reach steady state conditions. Three decades later, Eskilson (1987) propose the finite line source model (FLS) which account for axial effects and gets rid of the previous limitation. These analytical approaches, however, only consider heat transfer by conduction and the natural groundwater flow is not accounted for. Chiasson et al (2000) was one of the first researchers to evaluate numerically the effect on groundwater flow on the heat transfer at the BHE. Later, Sutton et al. (2003) and Diao et al. (2004) propose the moving infinite line source model (MILS); an analytical solution that accounts for groundwater flow.

Analytical approaches combining groundwater flow and axial effects on the heat transfer of BHE have not been proposed yet. This problem is discussed in Chapter 4. Additionally, the effect of thermal dispersion on temperature plumes produced by GSHP systems is evaluated in Chapter 5. The latter might be important for regulation and monitoring of this kind of systems.

2.2. Natural temperature variations as hydrogeological tracer

Temporal variations of temperature serve as a natural tracer that can be applied in hydrogeological interpretation. They can be used to evaluate groundwater-surface water interaction and to determine hydraulic parameters of the underground by coupling groundwater flow and heat transport models (Stallman 1965). Additionally, heat as a tracer is useful for instance for the delineation of flow and resident times in the hyporheic zone (Anderson 2005), as well as for the analysis of spatial and temporal dynamics of chemical loading to a river or aquifer.

Numerical models are widely applied to simulate surface water – groundwater interaction based on measured groundwater temperatures (Barlow and Coupe 2009; Bense and Kooi 2004; Blasch et al. 2006; Bravo et al. 2002; Bundschuh 1993; Constantz et al. 2002; Duque et al. 2010; Lapham 1989; Niswonger et al. 2005; Su et al. 2004; Ronan et al. 1998). Lapham (1989), for instance, investigated

vertical flow rates in sediments beneath streams. He solved the partial differential equation given by Stallman (1965) in one dimension (1D) under transient conditions by means of an explicit finite-difference numerical method. In related studies on surface water – groundwater interaction, the flow and heat transport code VS2DH was used for 1D (Blasch et al. 2006; Constantz 1998; Constantz et al. 2002; Barlow and Coupe 2009) and 2D simulations (Niswonger et al. 2005; Ronan et al. 1998; Su et al. 2004; Duque et al. 2010). Bundschuh (1993) employed the code SUTRA to evaluate the influence of the seasonal temperature fluctuations at the surface on the temperature of the aquifer. Bravo et al. (2002) used the code HST3D to estimate ground water discharge into the wetland and aquifer hydraulic conductivity.

Such numerical models are suitable for heterogeneous media, complex configurations and boundary conditions. Alternatively, as long as simple configurations are studied and homogeneous aquifers can be assumed, analytical solutions are favorable. They can be fast and straightforward means to quantify surface water infiltration rates based on temperature measurements (Bredehoeft and Papaopulos 1965; Goto et al. 2005; Hatch et al. 2006; Keery et al. 2007; Stallman 1965; Suzuki 1960; Taniguchi 1993).

From the aforementioned discussion, it is noticeable that numerical and analytical models have been applied to evaluate temperature transport in aquifers under the influence of surface temperatures fluctuations. However, conceptual simplifications of the subsurface such as conduction into confining layers have not been examined in detail yet. Therefore, Chapter 3 presents a concise evaluation and discussion about it.

3. Paper I:

Propagation of seasonal temperature signals into an aquifer upon bank infiltration[1]

Abstract: Infiltrating river water carries the temperature signal of the river into the adjacent aquifer. While the diurnal temperature fluctuations are strongly dampened, the seasonal fluctuations are much less attenuated and can be followed into the aquifer over longer distances. In one-dimensional model with uniform properties, this signal is propagated with a retarded velocity, and its amplitude decreases exponentially with distance. Therefore, time shifts in seasonal temperature signals between rivers and groundwater observation points may be used to estimate infiltration rates and near-river groundwater velocities. As demonstrated in this study, however, the interpretation is non-unique under realistic conditions. We analyze a synthetic test case of a two-dimensional cross-section perpendicular to a losing stream, accounting for multi-dimensional flow due to a partially penetrating channel, convective-conductive heat transport within the aquifer, and heat exchange with the underlying aquitard and the land surface. We compare different conceptual simplifications of the domain in order to elaborate on the importance of different system elements. We find that temperature propagation within the shallow aquifer can be highly influenced by conduction through the unsaturated zone and into the underlying aquitard. In contrast, regional groundwater recharge has no major effect on the simulated results. In our setup, multi-dimensionality of the flow field is important only close to the river. We conclude that over-simplistic analytical models can introduce substantial errors if vertical heat exchange at the aquifer boundaries is not accounted for. This has to be considered when using seasonal temperature fluctuations as a natural tracer for bank infiltration.

[1] Molina-Giraldo, N., P. Bayer, P. Blum, and O.A. Cirpka. 2011. *Ground Water* 49 no. 4: 491–502.

3.1. Introduction

A surface-water body that infiltrates into an aquifer also influences the subsurface temperature regime. Temporal fluctuations of temperature have been recognized as a natural tracer that may be used for hydrogeological interpretation (Suzuki 1960; Stallman 1965; Lapham 1989; Constantz 1998; Conant 2004; Blasch et al. 2006; Hoehn and Cirpka 2006; Keery et al. 2007; Duque et al. 2010; Vogt et al. 2010, among others; Anderson 2005; Hatch et al. 2006). Natural temperature variations are attractive tracers, because they are intrinsic to the system. In contrast to synthetic tracers in well-to-well or river-to-well applications, no additional injection campaigns are necessary, thus avoiding alterations of the natural flow regime and groundwater chemistry (Constantz et al. 2003). Furthermore, none of the regulative constraints that may apply for conventional tracers, such as fluorescent dyes, have to be considered. Finally, groundwater temperature can easily be measured over long time periods in monitoring wells by means of relatively inexpensive thermometers, commonly included in water-level loggers (e.g., Stonestrom and Blasch 2003; Ma and Zheng 2010; Anderson 2005).

Variation of radiation and air temperature causes fluctuation of surface-water temperatures. Typically, the most pronounced signals are related to diurnal and seasonal changes of short-wave radiation triggered by the path of the sun. These periodic signals are superimposed by variations on the time scale of several days caused by synoptic weather phenomena. The temperature signals are transmitted from the surface-water body into a connected aquifer by conduction and convection. The latter denotes heat transport by the moving water. Mixing processes due to microscale differential groundwater velocity and macroscale geological heterogeneities create thermal dispersion (Bear 1972). Heat transfer by conduction is governed by the temperature gradient. Accordingly, the dominant processes are convection at high infiltration rates, and conduction in parts of the subsurface with slowly flowing or even stagnant water.

As the temperature signal penetrates into the aquifer, it is dampened (i.e., the amplitude is attenuated) and shifted in time. As an illustrative example, Figure 3-1 shows the temperature time series measured

in the losing River Thur, Switzerland, and an observation well at about 50 m distance. Details of the corresponding field study are described by Cirpka et al. (2007). The river time series exhibits a seasonal trend, which can be approximated well by a sinusoidal function with amplitude of about 8 K. The river signal also includes diurnal variations (amplitude of about 2 K in the summer), which are graphically not well resolved in Figure 3-1. Apparently, the groundwater time series of the observation well has lost the diurnal signal, whereas the seasonal variation is hardly dampened and slightly shifted towards later times. Hence, after some travel distance the remaining temperature signal is the seasonal one.

The time series of Figure 3-1 are representative for losing rivers and associated alluvial aquifers in middle latitudes, with considerable annual temperature variations and substantial infiltration. The degree of dampening depends on the groundwater flow velocity, the thermal diffusivity, and the frequency of the temperature signal (Stallman 1965). High-frequency (e.g., diurnal) temperature fluctuations are more dampened than low-frequency (e.g., seasonal) ones, because the related spatial temperature profiles have larger gradients, even with identical amplitudes. Typically, diurnal temperature signals become undetectable at infiltration distances that are considerably larger than 1 m. In recent years, the analysis of these signals in vertical profiles within river beds has been used in various studies to estimate local exchange rates of water in both losing and gaining streams (e.g., Keery et al. 2007; Vogt et al. 2010; Constantz 2008; Hatch et al. 2006). The method requires measurement equipment to be installed within the river on a mostly temporary basis, because it would not withstand mechanical stresses during floods.

In contrast to diurnal fluctuations, seasonal temperature signals may penetrate to distances of tens to hundreds of meters and can therefore be detected in standard piezometers equipped with thermometers in the vicinity of the river, like in the case depicted in Figure 3-1. In theory, seasonal temperature fluctuation might therefore be used to infer residence times of water and flow rates in alluvial aquifers, which are required for planning of freshwater extraction wells close to rivers. However, Hoehn and Cirpka (2006) warned that the interpretation of seasonal temperature variations as natural tracers for bank infiltration may be impeded by interference with seasonal temperature signals from sources other than the infiltrating river water. They were mainly arguing that several water streams of shallow origin may mix within the subsurface.

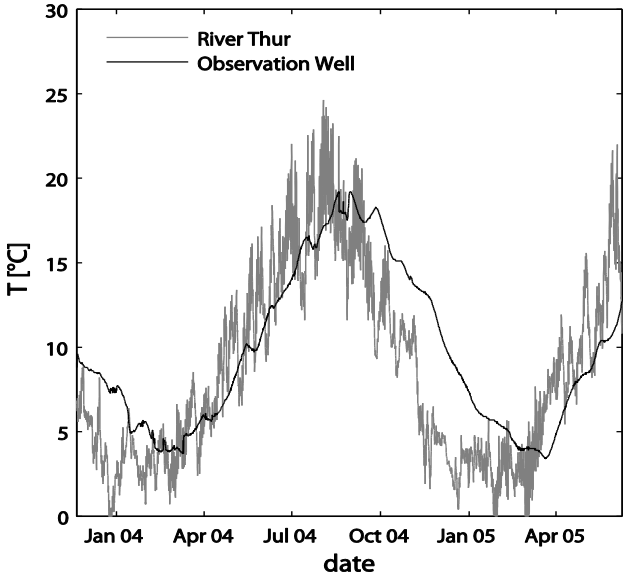

Figure 3-1. Temperature time series of 2004-2005 measured in the River Thur, Switzerland, and in an adjacent groundwater observation well in 50 m distance to the river (Cirpka et al. 2007).

The objective of this study is to examine in detail how the seasonal temperature signal of a river is propagated into an adjacent aquifer. In particular, we want to elucidate to what extent a unique interpretation from measurements in individual groundwater observation wells is possible. A synthetic case is defined with a river that continuously infiltrates into an aquifer with an overlying unsaturated zone and an underlying aquitard. The set up is based on a typical alluvial aquifer with shallow water table and small aquifer thickness (e.g., Hoehn and Cirpka 2006; Riva et al. 2006). Simulations are performed for an idealized vertical cross-section in the general groundwater flow direction. While applications of numerical models for temperature transport in aquifers influenced by surface-water bodies have been presented in several studies (e.g., Lapham 1989; Bundschuh 1993; Bravo et al. 2002; Niswonger and Prudic 2003; Bense and Kooi 2004; Su et al. 2004; Blasch et al. 2006; Duque et al. 2010; Barlow and Coupe 2009; Constantz et al. 2002; Ronan et al. 1998), the purpose of the current work is to analyze how conceptual simplifications of the surface and subsurface, such as recharge, multi-dimensionality of the flow field due to a partially penetrating channel, and conduction into the aquitard and the top layer, impact the accuracy of the simulations of temperature fluctuations.

3.2. Mathematical Model

3.2.1. Governing Equations

In the synthetic study case, we consider steady-state groundwater flow without internal sources and sinks following the standard groundwater flow equation (Bear 1972; de Marsily 1986):

$$\nabla \cdot (K \nabla h) = 0 \tag{3-1}$$

subject to the following boundary conditions:

$$h = \hat{h} \text{ on } \Gamma_1 \tag{3-2}$$

$$(K \nabla h) \cdot \mathbf{n} = \hat{q} \textbf{ on } \Gamma_2 \tag{3-3}$$

where h denotes the hydraulic head, and K is the hydraulic conductivity assumed isotropic; $\hat{h}$ and $\hat{q}$ are prescribed values of the hydraulic head at boundary Γ_1 and the normal inwardly directed flux at boundary Γ_2, respectively; **n** is the unit normal vector pointing outwards. For the unsaturated zone, the effective saturation and unsaturated hydraulic conductivity are computed using the van-Genuchten-Mualem parameterization (van Genuchten 1980):

$$S_e(h_c) = \left(1 + (\alpha h_c)^N\right)^{\frac{1-N}{N}} \tag{3-4}$$

$$K(h_c) = K_{sat} \sqrt{S_e} \left(1 - \left(1 - S_e^{\frac{N}{N-1}} \right)^{\frac{N-1}{N}} \right)^2 \tag{3-5}$$

in which S_e denotes the effective water saturation, α and N are the van-Genuchten parameters depending on the soil type, and K_{sat} is the saturated hydraulic conductivity. The capillary head (h_c), is calculated as follows:

$$h_c = \min(z - h, 0) \tag{3-6}$$

where z is the elevation above a reference datum and h is the hydraulic head referenced to the same datum.

Heat transport in porous media is expressed by the convection-dispersion equation, written here in a form that is formally identical to the advection-dispersion equation for solute transport (de Marsily 1986; Domenico and Schwartz 1998):

$$\frac{\partial T}{\partial t} + \nabla \cdot (\mathbf{v}_{\mathrm{T}} T) - \nabla \cdot (\mathbf{D} \nabla T) = 0 \tag{3-7}$$

in which T denotes temperature, t is time, $\mathbf{v}_{\mathrm{T}}$ is the effective velocity of convective heat transport, and $\mathbf{D}$ is the dispersion tensor for conductive-dispersive heat transfer. For heat transfer, the boundary Γ of the domain is subdivided into the inflow section Γ_{in} and a fixed-temperature section Γ_{fix}, both at which we assume a known temperature value, and the remaining part $\Gamma \backslash (\Gamma_{in} \cup \Gamma_{fix})$ across which the conductive-dispersive heat transport is set to be zero:

$$T = \hat{T}_0(t) \qquad \textbf{on} \quad \Gamma_{in} \cup \Gamma_{fix} \tag{3-8}$$

$$(\mathbf{D} \nabla T) \cdot \mathbf{n} = 0 \qquad \textbf{on} \quad \Gamma \backslash (\Gamma_{in} \cup \Gamma_{fix}) \tag{3-9}$$

in which $\hat{T}_0(t)$ is the temperature at $\Gamma_{in} \cup \Gamma_{fix}$. In our application, $\hat{T}_0(t)$ varies periodically in time.

The temperature dispersion tensor $\mathbf{D}$ is parameterized as follows (Bear 1972):

$$D_{ij} = \frac{v_{\mathrm{T}i} v_{\mathrm{T}j}}{\|\mathbf{v}_{\mathrm{T}}\|} (\alpha_x - \alpha_y) + \delta_{ij} \left(\frac{\lambda_m}{\rho_m c_m} + \alpha_y \|\mathbf{v}_{\mathrm{T}}\| \right) \tag{3-10}$$

where α_x and α_y are the longitudinal and transverse thermal dispersivities, respectively, λ_m is the thermal conductivity, $\rho_m c_m$ is the volumetric heat capacity of the porous medium, and δ_{ij} is the Kronecker delta-function which is one for $i = j$ and zero otherwise.

The effective thermal velocity of convective heat transport $\mathbf{v}_{\mathrm{T}}$ is related to specific discharge $\mathbf{q}$ and the seepage velocity of conservative solute transport $\mathbf{v}_a$ as follows:

$$\mathbf{v}_{\mathrm{T}} = \frac{\mathbf{q} \rho_w c_w}{\rho_m c_m} = \mathbf{v}_a \frac{\theta \rho_w c_w}{\rho_m c_m} = \frac{\mathbf{v}_a}{R_{\mathrm{T}}} \tag{3-11}$$

where $\rho_w c_w$ is the volumetric heat capacity of water, and θ is the porosity. R_T denotes the ratio of seepage velocity to effective thermal velocity of heat transport, also known as retardation factor of temperature, which is given as the ratio between the volumetric heat capacities of the porous medium, $\rho_m c_m$ and water $\Theta_w \rho_w c_w$ in which Θ_w is the volumetric water content. The volumetric heat capacity of the bulk porous medium is computed as the weighted arithmetic mean of the solids ($\rho_s c_s$) and water ($\rho_w c_w$) (Domenico and Schwartz 1998; Anderson 2005). The contribution of the gas phase is ignored due to its low density:

$$\rho_m c_m = \Theta_w \rho_w c_w + (1-\theta)\rho_s c_s \tag{3-12}$$

The volumetric water content (Θ_w) can be computed as follows (van Genuchten 1980):

$$\Theta_w = S_e \left(\Theta_{sat} - \Theta_r\right) + \Theta_r \tag{3-13}$$

where Θ_r and Θ_{sat} are the values of residual and saturated volumetric water content.

The weighted geometric mean of the thermal conductivity of the solids (λ_s), water (λ_w) and gas phase (λ_g) is used to calculate the thermal conductivity λ_m of the bulk porous media in the unsaturated zone (Nield and Bejan 2006):

$$\lambda_m = \lambda_s^{1-\theta} \lambda_w^{\Theta_w} \lambda_g^{\theta-\Theta_w} \tag{3-14}$$

3.2.2. Analytical Solution in One Spatial Dimension

If possible, it is desirable to use fast and straightforward analytical solutions. Most of the analytical approaches available to determine infiltration rates based on temperature measurements follow the works by Suzuki (1960), Stallman (1965) and Bredehoeft and Papadopulos (1965). Stallman (1965) extended the analytical solution given by Suzuki (1960) for computing infiltration and exfiltrating rates under transient conditions and periodic boundary conditions. Bredehoeft and Papadopulos (1965) presented a steady-state analytical solution for calculating vertical rates of groundwater movement. Taniguchi (1993), Goto et al. (2005), Hatch et al. (2006) and Keery et al. (2007), among others, used Stallman's (1965) analytical expression to calculate vertical groundwater fluxes based on periodic surface temperature fluctuations. All of these 1-D analytical solutions are restricted to special

conditions in which heat transfer between the periodic temperature boundary and the observation point can be approximated by strictly one-dimensional convective-dispersive transport.

The Fourier transform (see Appendix A) of equation (3-7) in a 1-D system with uniform properties reads as:

$$2\pi if\tilde{T} + v_{\mathrm{T}} \frac{\partial \tilde{T}}{\partial x} - D \frac{\partial^2 \tilde{T}}{\partial x^2} = 0 \tag{3-15}$$

subject to the boundary conditions:

$$\tilde{T}(x = 0, t) = \tilde{T}_0(f) \tag{3-16}$$

$$\tilde{T}(x = \infty, t) = 0 \tag{3-17}$$

The solution for equation (3-15) to equation (3-17) is an exponential function with complex argument:

$$\tilde{T}(x, f) = \tilde{T}_0(f) \exp(-kx) \tag{3-18}$$

in which k denotes a complex decay coefficient:

$$k(f) = \frac{\sqrt{v_T^2 + 8\pi ifD} - v_T}{2D} \tag{3-19}$$

Substituting equation (3-18) into the back Fourier transform of equation (A-1) yields:

$$T(x,t) = \int_{-\infty}^{\infty} \tilde{T}_0(f) \exp(-k(f)x) \exp(2\pi ift) \mathrm{d}f \tag{3-20}$$

Splitting k into its real (k_R) and imaginary (k_I) components, results in the following two equations:

$$T(x,t) = \int_{-\infty}^{\infty} \tilde{T}_0(f) \exp(-k_R x) \exp\left(2\pi if\left(t - \frac{x}{c_{wave}}\right)\right) \mathrm{d}f \tag{3-21}$$

$$c_{wave} = \frac{2\pi f}{k_I} \tag{3-22}$$

where c_{wave} is the celerity of the sinusoidal wave propagation. Finally, considering the specific case of a sinusoidal temperature signal $T_0(t)$ with amplitude a_T and the phase shift ϕ,

$$T_0(t) = a_T \cos(\phi + 2\pi ft) \tag{3-23}$$

The solution in the time domain is as follows (Stallman 1965):

$$T(x,t) = a_T \exp(-k_R x) \cos\left(\phi + 2\pi f\left(t - \frac{x}{c_{wave}}\right)\right) \tag{3-24}$$

3.2.3. Numerical Simulation in a Vertical Cross-Section

In order to account for more complex processes and geometries than realized by standard analytical methods, numerical simulation is needed. In the present work, the Finite Element Method (FEM) is utilized to solve the governing equations in two spatial dimensions. A vertical cross-section of an alluvial aquifer adjacent to a river is simulated in detail. The standard Galerkin method is used to simulate the groundwater flow equation (equation (3-1)) and the Streamline-Upwind Petrov-Galerkin (SUPG) method (Brooks and Hughes 1982) is applied to the heat transport equations in the Fourier domain (equations (A-6) and (A-7)). A uniform grid of bilinear rectangular elements of constant coefficients discretizes the cross section. Each grid element has 0.1 m height and 1 m length. The model output is the spatial field of the Fourier-transformed temperature $\tilde{T}$, which is a complex number. The magnitude and the angle of the complex temperature represent the amplitude (a_T) and the phase shift (ϕ) of the periodic temperature signal:

$$a_T = \left\|\tilde{T}\right\| \tag{3-25}$$

$$\phi = \tan^{-1}\left|\frac{\mathrm{Re}(\tilde{T})}{\mathrm{Im}(\tilde{T})}\right| \tag{3-26}$$

3.3. Model Setup

The study case represents a straight river with vertical and lateral infiltration. Seven model variants of different complexity are set up to examine the role of different conceptual assumptions (Figure 3-2). They are used to simulate temperature changes in the aquifer due to infiltration and hence are all

oriented perpendicular to the river. Note that for strongly meandering rivers and even for straight rivers with a component of groundwater flow parallel to the channel, the assumption of essentially two-dimensional flow might not be valid (Woessner 2000). We start with a full model (Scenario 1) accounting for conductive/dispersive and convective heat transfer in the groundwater flow field, conductive heat transfer into an underlying aquitard and an unsaturated zone on top. For the latter, heat parameters depend on the volumetric water content as denoted by equations (3-12) and (3-14). The full model also simulates convective heat transfer by groundwater recharge, and seasonal fluctuations of the surface and river temperature. The geothermal heat flux is not considered because it is constant in time. Each of the listed processes adds additional complexity to the model and so the question is which components might be neglected while still arriving at valid temperature predictions in the aquifer. To answer this, the full model is simplified by eliminating groundwater recharge (scenario 2), multi-dimensionality of the flow field and hence assuming a fully penetrating channel (scenario 3), conduction in the aquitard (scenario 4), heat transfer in the top layer (scenario 5), and also a combination of the last two (scenario 6). The resultant six different model conceptualizations are numerically solved in 2-D in the Fourier domain. The simplest model (scenario 7) is the representation of the aquifer as a one-dimensional column connected to the river, which is simulated using the analytical expression by Stallman (1965) (equation (3-24)).

The full model (scenario 1) is considered the most accurate and thus serves as a reference to be compared with the other scenarios. As a criterion, the root mean square error (RMSE) is selected, which quantifies the residual error of the temperature evolution in the aquifer between the full model and the simplified ones. The RMSE is applied to the complex temperature as follows:

$$\mathrm{RMSE} = \sqrt{\frac{1}{2A_{aq}} \int_{A_{aq}} \left\{\mathrm{Re}(T_1(x) - T_2(x))\right\}^2 + \left\{\mathrm{Im}(T_1(x) - T_2(x))\right\}^2 \mathrm{d}x} \qquad (3\text{-}27)$$

in which A_{aq} is the cross-sectional area of the aquifer within the model plane.

Similar boundary conditions to scenario 1 and 2 were used by Bundschuh (1993) and Duque et al. (2010). The latter evaluated the surface water-groundwater interaction by a heat-tracer test using the heat-transport code VS2DHI (Healy and Ronan 1996). Bundschuh (1993) applied the USGS code SUTRA (Voss 1984) to evaluate the influence of the seasonal temperature fluctuations at the surface on the temperature of the aquifer.

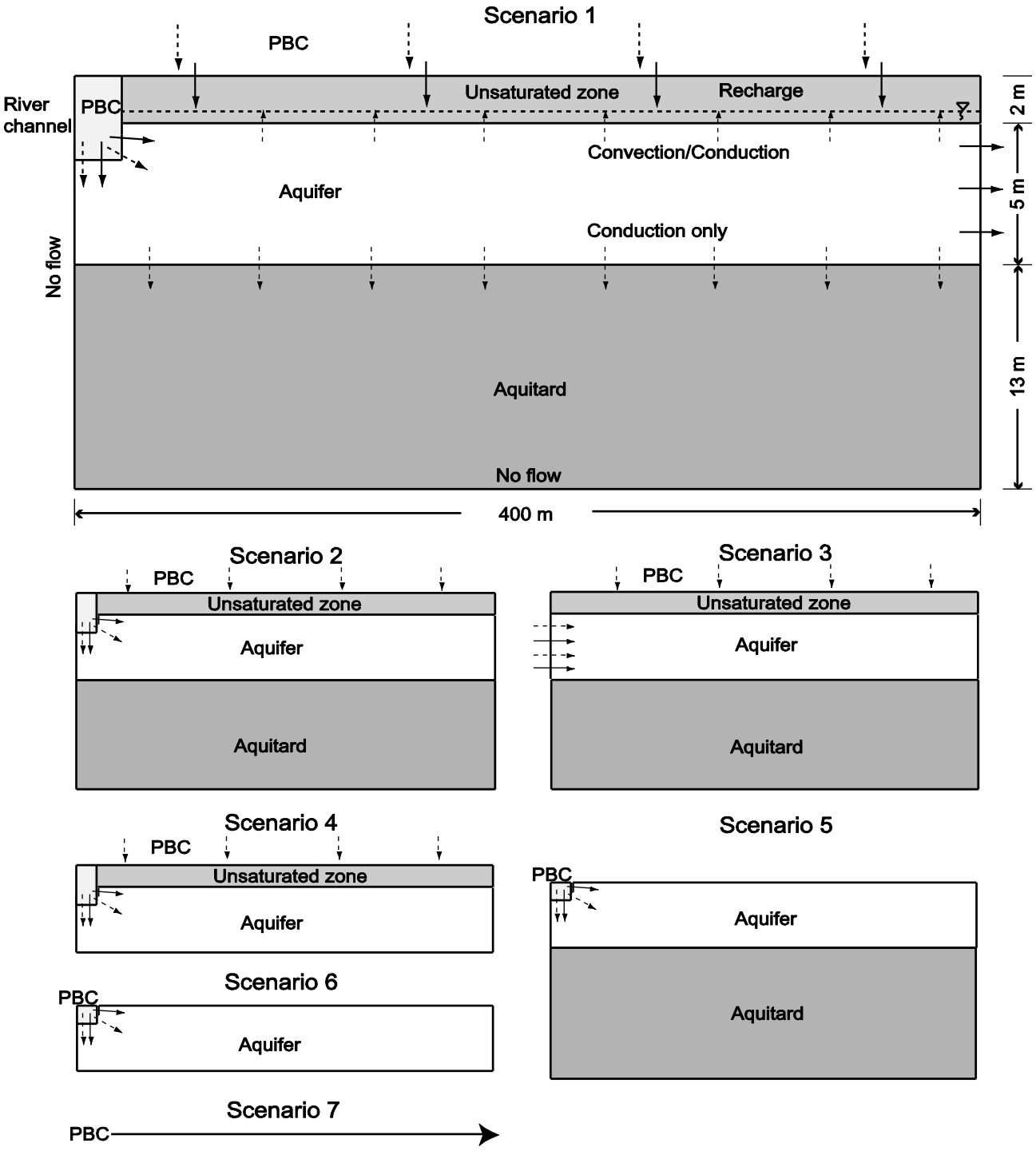

Figure 3-2. Model setups of different complexity. Scenario 1 (full model), 2 (without recharge), 3 (fully penetrating channel), 4 (without aquitard), 5 (without unsaturated zone), 6 (only aquifer) and 7 (1-D analytical solution). PBC: Temperature periodic boundary conditions; dashed arrow: heat transfer (convection and conduction); solid arrow: water flow.

3.3.1. Boundary Conditions and Aquifer Geometry

Scenario 1 (full model) is built of three horizontal layers (Figure 3-2). The upper layer (sandy loam) represents the unsaturated zone, the middle layer (sandy gravel) the aquifer, and the bottom layer (clay) the aquitard. Many alluvial aquifers exhibit a small distance to groundwater and a small aquifer thickness (e.g., Hoehn and Cirpka 2006; Riva et al. 2006). Accordingly, the thickness of the unsaturated zone is set to 2 m and that of the aquifer to 5 m. A thickness of 13 m is assigned to the aquitard to minimize boundary effects by the model bottom while including heat conduction into the aquitard. A preliminary analysis showed that for larger aquitard thicknesses the results do not change considerably. The horizontal length of the model domain is set to be 400 m. However, different lengths are also inspected in order to evaluate the effect of the scale of the model domain. No-flow boundary conditions are applied to the left and bottom boundary. Half of the river channel (10 m) is implemented at the upper left boundary. The other half of the river channel is assumed to be symmetrical

A constant head in the river is assumed. The rationale for this assumption is that the fluctuations of the river stage and infiltration rates average out on the seasonal time scale considered here. This may be representative for rivers where the water level is regulated (e.g., by reservoirs), or for humid climates where water level fluctuations of the river throughout the year are small. Accordingly, the presented approach may only yield approximate results for cases with strong variation of infiltration rates.

In the model, fixed-head boundary conditions are applied to the river and the right model face. The water enters the aquifer by infiltration through the river bed and the groundwater leaves the domain through the right boundary in the aquifer. A uniform regional recharge rate of 300 mm per year is allocated to the top boundary, which is a typical value of groundwater recharge in central Europe (Langguth and Voigt 2004). Fourier transformation in time is used to evaluate the periodic boundary conditions at the river and the top boundary. The temperature fluctuations are specified by an amplitude of 8 K and a frequency of 1/year.

3.3.2. Aquifer Parameters

Hydraulic and thermal aquifer parameters used in the simulation are typical for sandy aquifers. Values are listed in Table 3-1. Due to the low variability of thermal parameters compared with hydraulic parameters, the same values of the thermal conductivity and heat capacity are used for the three

horizontal layers. The hydraulic conductivity values listed in Table 3-1 are for saturated sediments. The resulting groundwater velocity in the aquifer is ≈ 1 m/day assuming a hydraulic gradient of 3 ‰. The aquifer system is assumed to be isotropic with respect to hydraulic conductivity. The effects of buoyancy and changes in viscosity are neglected. Therefore, the hydraulic and thermal parameters are assumed to be independent of the temperature changes. The effect of density and viscosity in heat transport problems for shallow aquifers is discussed, for example, by Hecht-Méndez et al. (2010), and Ma and Zheng (2010). The latter stated that variable density and viscosity due to temperature changes of less than 15 K seem to be negligible in the flow model. In the present study, an atmospheric temperature change of 16 K is assumed between winter and summer. Nevertheless, at any given time, the temperature variability within the model domain is not larger than 10 K.

Table 3-1. Hydraulic and thermal parameters used in the simulations (de Marsily 1986; Carsel and Parrish 1988; Spitz and Moreno 1996).

Parameter	Value
Specific heat capacity of solids [J/kg/K]	880
Specific heat capacity of water [J/kg/K]	4190
Density of the solids [kg/m^3]	2650
Thermal conductivity of solids [W/m/K]	2.00
Thermal conductivity of water [W/m/K]	0.58
Thermal conductivity of gas phase [W/m/K]	0.025
Total porosity [-]	0.30
Longitudinal dispersivity [m]	1.0
Transverse dispersivity [m]	0.01
Hydraulic gradient [‰]	3
Saturated hydraulic conductivity [m/s]	
Aquifer	1.0×10^{-3}
Aquitard	1.0×10^{-10}
Unsaturated zone	1.0×10^{-6}
van Genuchten parameters	
α [1/m]	3.6
N	1.56

3.4. Results and Discussion

3.4.1. Full Model Simulations

Results for the full model (scenario 1) are obtained numerically in 2-D in the Fourier domain. Figure 3-3 depicts the calculated spatial distribution of the seasonal temperature amplitude. The temperature signal originating from the river is propagated over the entire aquifer thickness close to the river and over a distance of approximately 90 m. Further away from the river, the signal originating from the

surface is almost completely dampened in the unsaturated zone and in the first top meter of the aquifer. The degree of dampening of the temperature signals is linked to the groundwater flow velocity, the thermal diffusivity, and the frequency of the temperature signal. The penetration distance of the temperature signal is the distance at which the temperature amplitude in the subsurface has fallen to e^{-1} (i.e., 37%) compared to that of the periodic signal at the surface (Goto et al. 2005; Vogt et al. 2010). From equation (3-24), the penetration distance (x_p) of the temperature front in a 1-D system is therefore defined as $1/k_R$, which can be expressed as follows:

$$x_p = \frac{2D}{\sqrt{\left(v_T^2/2\right)+\sqrt{\left(v_T^4/4\right)+16\pi^2 f^2 D^2}}-v_T} \tag{3-28}$$

In case of zero convection equation (3-28) simplifies to:

$$x_p(v_T = 0) = \sqrt{\frac{D}{\pi f}} \tag{3-29}$$

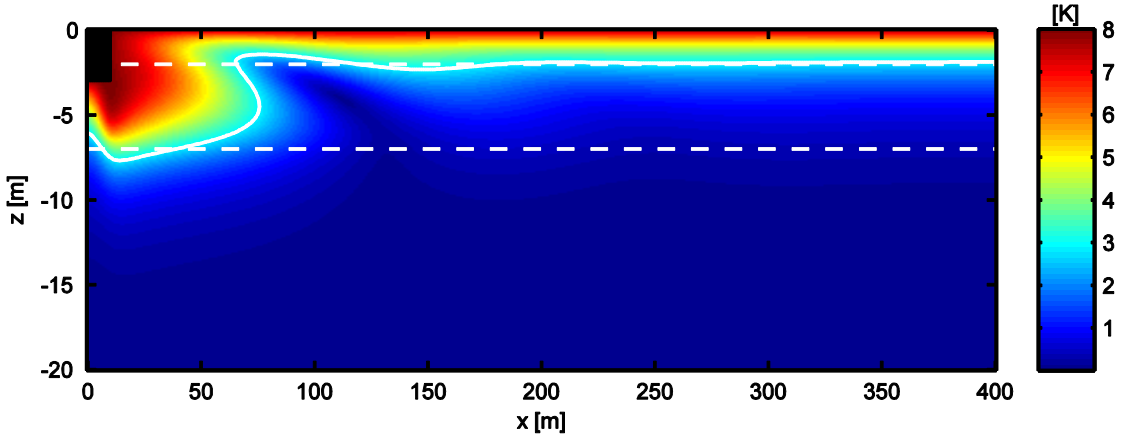

Figure 3-3. Simulated amplitude of the seasonal temperature signal for the full model (Scenario 1). The river is located in the upper left corner. Dashed white lines: top and bottom of the aquifer; solid white line: penetration distance defined by an amplitude of $a_T \times \exp(-1) \approx 2.94$ K.

Assuming the unsaturated zone as a 1-D problem in the vertical direction, the computed penetration depth in the unsaturated zone for the full model is about 2 m for seasonal fluctuations. In contrast, for diurnal fluctuations the vertical temperature signal is almost completely dampened in the first 0.20 m. We can conclude that although the seasonal temperature signal originating from the surface is strongly dampened through the unsaturated zone, it could still have an effect on the aquifer temperature depending on the thickness of the unsaturated zone.

Figure 3-4 shows the time shift or apparent travel time of temperature. The time shift in Figure 3-4a is plotted based on the wrapped phase shift. Therefore, the time shift is restricted to cycles of 1 year. In comparison, Figure 3-4b presents the results after correcting the phase shift by adding multiples of 2π in order to obtain a continuous function (unwrapped time shift) of apparent travel times of temperature.

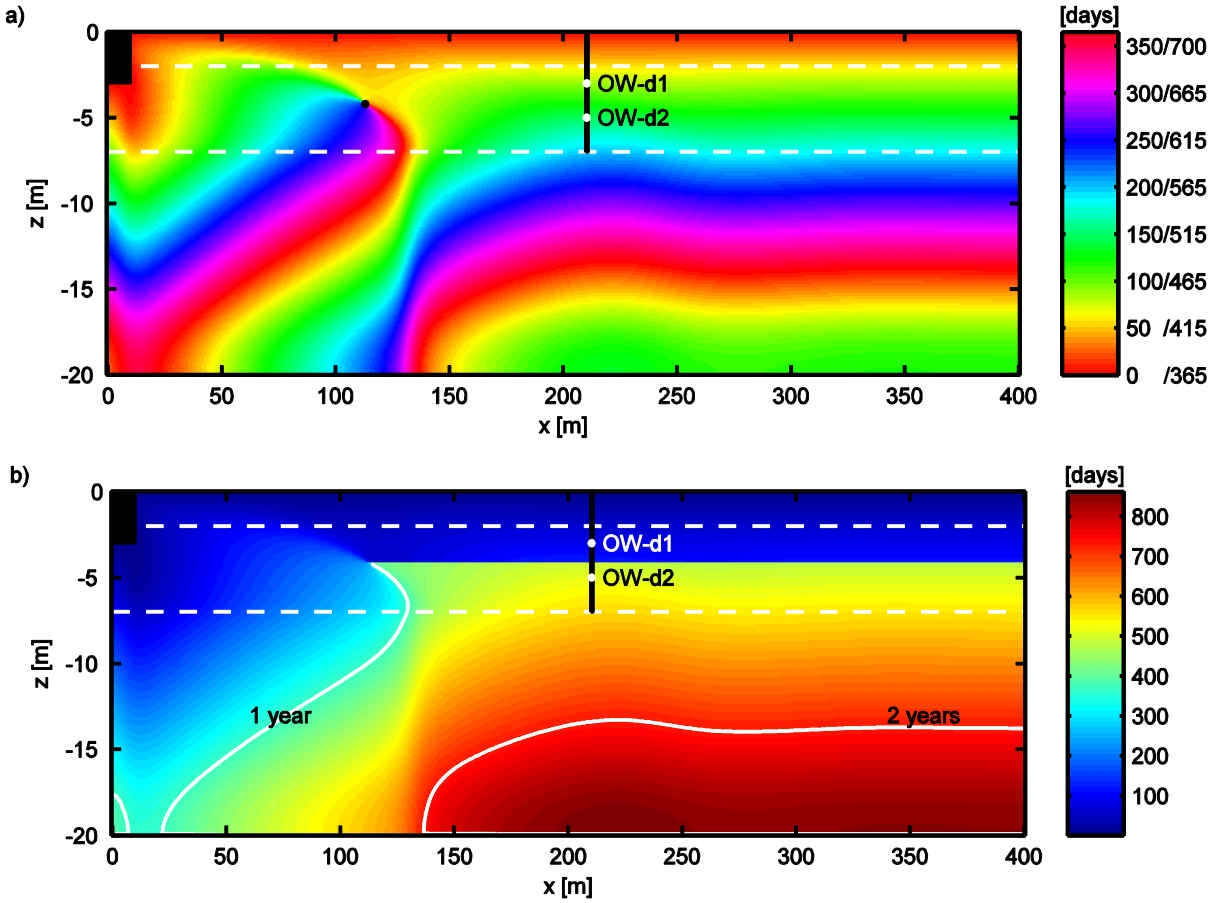

Figure 3-4. a) Wrapped time shift; b) Unwrapped time shift (true isochrones). The river is located in the upper left corner. Dashed white lines: top and bottom of the aquifer; solid white lines: time shift of 1 year and 2 years; black point: location where the amplitude is zero.

Evidently, Figure 3-4a can result in misinterpretations of the apparent travel times of temperature due to the wrapped phase shift. A mismatch by multiples of 1 year can occur depending on the point of view the time shift profile is observed. Consider the following example: A hypothetical observation well is located 200 m away from the river and two measuring points of groundwater temperature are placed at 3 m (OW-d1) and 5 m (OW-d2) depth (Figure 3-4). The time shift observed at the 5 m depth point can be either 120 days or 485 days, depending on the interpretation. For a vertical profile starting at the ground surface, the travel time of temperature would be misinterpreted as 120 days. For a longitudinal profile starting at the left boundary of the model, the actual travel time of temperature is

485 days. At the 3 m depth point, an apparent temperature travel time of 85 days is identified. Assuming a retardation factor of 2.2, we get a residence time of water of 39 days, which is actually a measure of the signal originating mainly from the surface and not the river. Thus, interpretation of travel times based on seasonal signals originating from an infiltrating river might be affected by interference with additional sources of temperature fluctuations.

The black dot in Figure 3-4a marks a point where the interfering periodic signals originating from the river and from the surface cancel out, the amplitude is zero, and the time shift is not defined. It is intuitively clear that seasonal temperature time series observed at profiles downgradient of this point within the aquifer should not be interpreted by a simple 1-D analytical model. Figure 3-4a, however, also exemplifies that upstream of that point a substantial vertical profile of apparent travel time can be observed, either due to multi-dimensionality of the flow field (close to the river) or due to interference with conduction into the top and bottom layers (further away from the river).

3.4.2. Sensitivity Analysis of Individual Model Elements

In the following, the full model simulation (scenario 1) is compared with predictions from simplified models (Figure 3-2). Results based on the root mean square error (RMSE) as computed by equation (3-27) are listed in Table 3-2. It should be mentioned that the calculated error introduced by simplifying surface and subsurface process simulation is sensitive to the scale of the model domain. Hence, the errors are inspected for different lengths of the model cross section.

Table 3-2. RMSE of the Fourier-transformed temperature according to equation (3-27) [K]. Residual error of the temperature evolution in the aquifer between the full model and the simplified ones for different model lengths. Refer to Figure 3-2 for further details on the scenarios.

Length (m)	Scenarios					
	2	3	4	5	6	7
	Without recharge	Fully penetrating channel	Without aquitard	Without unsaturated zone	Only aquifer	1-D analytical solution
400	0.03	0.60	1.09	1.31	3.12	3.34
200	0.01	0.95	1.45	1.45	3.21	3.41
100	0.01	1.55	1.50	1.13	2.30	2.63
50	0.01	2.25	1.06	0.36	1.16	1.55
20	0.001	2.76	0.51	0.23	0.56	1.18

First we discuss the results for a model length of 400 m. The value of RMSE = 0.03 K for scenario 2 is small. Considering the amplitude of 8 K, this indicates that regional groundwater recharge is only of

minor importance for the simulation. This is mainly due to the low velocity of infiltration (10^{-9} m/s) compared with the average horizontal flow velocity of the aquifer (10^{-5} m/s). However, heat-transport simulation should be done with the awareness that errors could be introduced when neglecting groundwater recharge for higher recharge scenarios or during extreme hydrologic events depending on the hydrogeological setup.

Scenario 3 indicates that assuming a fully penetrating channel has a larger effect, but the RMSE is still below 1 K for a cross-section length of 400 m. Neglecting the conduction into the aquitard (scenario 4) yields a slightly higher RMSE of 1.09 K. The aquitard acts as a sink and source of heat. It stores heat during high-temperature periods and releases it during cold periods. Apparently, the aquitard needs much more attention in simulations of heat transport than in those of solute transport. This is mainly an effect of high thermal diffusion. Typical values of solute diffusion coefficients for small molecules are in the order of 10^{-9} m^2/s, whereas typical values for thermal diffusion coefficient are in the order of 10^{-7} m^2/s (Domenico and Schwartz 1998). Hence, diffusion into the underlying aquitards is of high relevance for the presented study case.

Removing the unsaturated zone (scenario 5) means that conduction into the unsaturated zone and seasonal temperature fluctuations at the land surface are ignored. This yields an error of about 1.30 K. In order to discriminate between these two factors, scenario 5 is also simulated including the unsaturated zone as the full model but without seasonal fluctuations at the surface. The result is a RMSE value of 1.0 K, and hence, the periodic boundary condition at the land surface significantly contributes to the error of scenario 5. Since the calculated errors highly depend on the chosen model geometry, general conclusions are difficult. For example, it can be expected that an increased thickness of the unsaturated zone mitigates the effect of the periodic temperature fluctuation of the top boundary on the aquifer temperature. Recall that the penetration depth for the presented model is about 2 m for seasonal fluctuations and that it is controlled by flow velocity, thermal diffusivity, and the frequency.

Once more, results for scenarios 6 and 7 highlight the limited value of model conceptualizations that neglect processes such as conduction into aquitard and unsaturated zone as well as temperature fluctuations at the land surface. Applying the simplified 1-D analytical equation even yields an error of 3.34 K. This is almost half of the applied amplitude of 8 K, and therefore the analytical model should be taken with caution for interpretation of seasonal temperature signals.

For shorter lengths of the model domain, the absolute errors change for each scenario, and the relative error contribution of the different model elements may vary. The shorter the model the more important the multi-dimensional flow component (close to the river) becomes. Shorter model domains imply a decrease of aquifer interfaces to the aquitard and unsaturated zone. Accordingly, the effects of temperature fluctuations at the surface and the conduction into the aquitard and unsaturated zone are less pronounced. For the specific conditions evaluated in this study, conduction through the top and bottom aquifer interfaces is only relevant at a distance of the observation well from the river of more than 50 m.

Figure 3-5 shows length profiles of the temperature amplitude and time shift averaged over the aquifer depth for the scenarios 1, 4, 5, and 7. Scenarios 2 and 3 show similar behavior to scenario 1, and scenario 6 is equivalent to scenario 7. Hence they are not shown in the figure. An extra 1-D scenario which only considers convection in the aquifer is also included. Figure 3-5a depicts the amplitude of the temperature signal as function of travel distance. After a threshold, at which the periodic signals originating from the river and the surface cancel out, the amplitude signal for scenarios 1 and 4 starts to oscillate due to the interaction between the two signals. This is in contrast to the simulations by scenarios 5 and 7, which do not account for seasonal temperature fluctuations at the surface. In these scenarios, the amplitude signal decreases exponentially with the travel distance from the river. Additionally, the amplitude signal is more dampened for scenarios 1, 4, and 5 than for scenario 7. This is attributed to the heat transfer with the underlying and overlying layers, which is simulated in scenarios 1, 4, and 5 but not in scenario 7.

Figure 3-5b shows the apparent travel time of the temperature signal as a function of distance to the river. Note that an overestimation of the time shift occurs if heat exchange with the land surface is neglected. The full model (scenario 1) clearly shows that the observed time shift between the river and depth-averaged groundwater signal of temperature is dominated by exchange with the land surface at large distances. At a sufficient distance, the apparent time shift does not vary with distance anymore. Scenario 4, in which the aquitard is neglected but the unsaturated zone and land surface are accounted for, shows a similar behavior. The models neglecting the unsaturated zone, by contrast, result in a monotonic increase of time shift with distance with the exception of very close distances to the river where multi-dimensionality of the flow field is important. Assuming no influence by temperature fluctuations at the land surface results in an underestimation of the time shift of temperature signals

(not shown in Figure 3-5) if conduction into the aquitard and unsaturated zone is neglected. This is in accordance with the fact that arrival time of the temperature front is delayed due to conduction processes into the overlying and underlying layers.

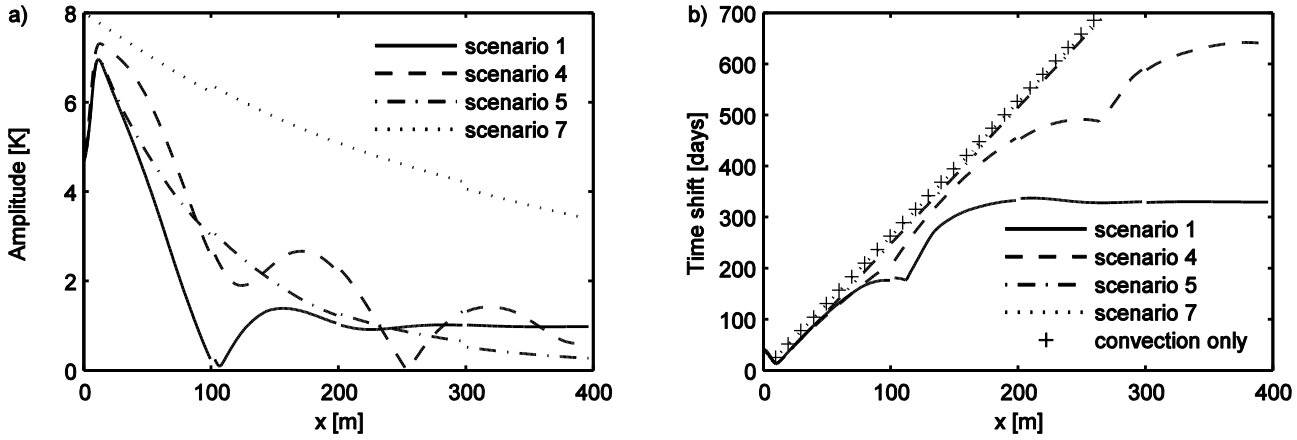

Figure 3-5. Longitudinal profiles of temperature amplitude (a) and time shift (b) averaged over the aquifer depth as function of distance to the river for scenarios 1 (full model), 4 (without aquitard), 5 (without unsaturated zone) and 7 (1-D analytical solution) as well as an extra scenario considering only convection.

In summary, Figure 3-5 shows that multi-dimensionality close to the river is important at distances of up to 10 m from the bank. In the given setup, the interpretation of time shifts by essentially all models is acceptable for distances between 10 m and 50 m. At larger distances, the model results start deviating. Downgradient of the point at which the two temperature signals cancel out (at about 110 m), interpretation of seasonal temperature signal by a model neglecting the heat exchange with the land surface is not possible. The exact location of this critical point depends on groundwater velocity, thickness of the unsaturated zone, and thermal conductivity. If in a field survey an almost complete disappearance of the seasonal temperature signal was observed in a dense transect of observation wells, there is only a minor chance of interpreting the reappearing seasonal signal to infiltrating river water. In practice, however, such dense transects are rare. That is, a single observation well at a distance of 150 m would exhibit a clear seasonal temperature signal with amplitude of 1 K that might be misinterpreted by mainly convective 1-D transport with too high velocity.

3.5. Conclusions

We have presented a modeling study to inspect the propagation of seasonal temperature signals from an infiltrating river into an adjacent aquifer. As key measures, we have considered the amplitude and time

shift of the seasonal temperature signal. In particular the latter would be used to estimate groundwater velocities from the time series. We have evaluated simplifications of physical processes in the model concept in order to assess which components of the modeled system have a major impact on the chosen measures.

In general, we can conclude that heat transfer by conduction from the aquifer into the unsaturated zone and into an underlying aquitard significantly influences the temperature signal distribution in a shallow aquifer. Arrival times of temperature signals at observation wells are underestimated when conduction into the overlying and underlying layers is neglected. The conduction into the aquitard causes additional attenuation of the seasonal temperature signal and a distinct vertical profile of the time shift. Conduction into the unsaturated zone would have identical effects if there was no influence by temperature fluctuations at the land surface. Interference of the signal originating from bank infiltration with that from the land surface leads to complex spatial patterns of amplitude and time shift, including a point at which both signals cancel out. This implies that a unique interpretation of apparent travel times from measurements of temperature time series in individual groundwater observation wells is often problematic. In the given context, a simple mismatch by multiples of 1 year may be the simplest cause of confusion, but the interference of different temperature signals can also cause non-integer offsets between simplistic 1-D simulations and the full model.

In our synthetic case study, the propagation of seasonal temperature fluctuations through the aquifer was not sensitive to regional groundwater recharge. This reflects the minor impact of convective heat transfer by groundwater recharge compared to conduction through the unsaturated zone and convection within the aquifer. The relative importance of convection by groundwater recharge would increase with a larger thickness of the unsaturated zone and larger distances to the river.

Multi-dimensionality of the flow field was important only at small distances to the river. At short travel distances, time shifts between temperature time series observed on observation wells to those of the river mainly reflect convective heat transport along the curvilinear flow path from the river to the observation point. Besides the difficulty of identifying this flow path, analyzing time series from observation points close to the river suffer from the small time shift. For a seasonal signal, an offset of at least one month is required to obtain a reasonable estimate of apparent travel times.

The geothermal heat flux has of course no effect on seasonal fluctuations because it does not vary on a seasonal time scale. In contrast, heat conduction from the aquifer into underlying aquitard can be of high relevance. In our setup, the most simplistic models that ignore the lateral heat-flux components yield significant residual errors over larger distances, indicating that these models become invalid for interpretation of measured temperature time series. There is a certain range of distances (in our setup between approximately 10 m and 50 m) in which the time shifts computed by the various models are similar. Only within this range the simplified models would be valid for interpretation of measured temperature time series.

Most current conceptualizations for the determination of bank infiltration and travel times from time series rely on 1-D analytical expressions or simplified numerical models. As pointed out, they are applicable only over a limited range of distances where assuming strictly one-dimensional convective-dispersive heat transfer between the river and the observation well is not introducing a severe bias. This range depends on groundwater velocity, that is, the very parameter to be estimated by the analysis, on the thickness of the aquifer and that of the unsaturated zone. Our general recommendation for practical applications is to perform simulations that include conduction into the over- and underlying layers as well as fluctuations of the land-surface temperature, such as our scenario 3, to test whether the model of an insulated 1-D tube is a valid simplification for the given travel distance. If a significant bias becomes evident, the analysis of the time series requires the more complex model.

Appendix A

Spectral representation

Usually, state variables are evaluated as function of space and time. Because we study time-periodic signals with frequency of one per year, it is convenient to transform the governing equations into the frequency domain by Fourier transformation. The Fourier transform of the time dependent temperature *T(t)* is defined as (Bracewell 2000):

$$\tilde{T}(f) = \int_{-\infty}^{\infty} T(t) \exp(-2\pi i t f) \mathrm{d}t \qquad \text{(A-1)}$$

with the frequency *f* and the imaginary number $i = \sqrt{-1}$. In general, $\tilde{T}$ is a complex number. Equation A-1 implies that the Fourier transform of the time derivative is:

$$\frac{\partial \tilde{T}}{\partial t} = 2\pi i f \tilde{T}(f) \tag{A-2}$$

Then, we can apply the Fourier transform to equation (3-7) and make use of orthogonality properties, resulting in a steady-state transport equation of the Fourier-transformed temperature $\tilde{T}$, which must be met for each frequency f ($\forall f$):

$$2\pi i f \tilde{T} + \nabla \cdot (\mathbf{v}_T \tilde{T}) - \nabla \cdot (\mathbf{D} \nabla \tilde{T}) = 0 \; \forall f \tag{A-3}$$

subject to the boundary conditions:

$$\tilde{T} = \tilde{\hat{T}}_0(f) \; \forall f \qquad \text{on} \quad \Gamma_{in} \tag{A-4}$$

$$(\mathbf{D} \nabla \tilde{T}) \cdot \mathbf{n} = 0 \; \forall f \qquad \text{on} \quad \Gamma \setminus \Gamma_{in} \tag{A-5}$$

in which $\tilde{T}$ depends on frequency f and space.

We may consider the real and imaginary contributions to equation (A-3) as a system of coupled equations:

$$-2\pi i f \, \mathrm{Im}(\tilde{T}) + \mathbf{v}_T \nabla \cdot (\mathrm{Re}(\tilde{T})) - \nabla \cdot (\mathbf{D} \nabla \, \mathrm{Re}(\tilde{T})) = 0 \; \forall f \tag{A-6}$$

$$2\pi i f \, \mathrm{Re}(\tilde{T}) + \mathbf{v}_T \nabla \cdot (\mathrm{Im}(\tilde{T})) - \nabla \cdot (\mathbf{D} \nabla \, \mathrm{Im}(\tilde{T})) = 0 \; \forall f \tag{A-7}$$

subject to:

$$\mathrm{Re}\left(\tilde{T}\right) = \mathrm{Re}\left(\tilde{\hat{T}}_0\right) \forall f \qquad \textbf{on} \quad \Gamma_{in} \tag{A-8}$$

$$\mathrm{Im}\left(\tilde{T}\right) = \mathrm{Im}\left(\tilde{\hat{T}}_0\right) \forall f \qquad \textbf{on} \quad \Gamma_{in} \tag{A-9}$$

$$(\mathbf{D} \nabla \, \mathrm{Re}(\tilde{T})) \cdot \mathbf{n} = 0 \; \forall f \qquad \textbf{on} \quad \Gamma \setminus \Gamma_{in} \tag{A-10}$$

$$(\mathbf{D} \nabla \, \mathrm{Im}(\tilde{T})) \cdot \mathbf{n} = 0 \; \forall f \qquad \textbf{on} \quad \Gamma \setminus \Gamma_{in} \tag{A-11}$$

Solving the convection-dispersion equation in the spectral domain provides the benefit of substituting the transient equation with a system of two steady-state equations. This can be done if a single sinusoidal signal is considered and hence $\tilde{\tilde{T}}$ is non-zero for only a single frequency *f*. In our case, this is $f=1/year$. For a boundary condition with arbitrary inflow temperature $\hat{T}_0(t)$, however, solving the convection-dispersion equation in the spectral domain provides hardly any benefit, since the integration in time is replaced by solving the spectral equation for all frequencies.

4. Paper II:

A moving finite line source model to simulate borehole heat exchangers with groundwater advection[2]

Abstract: Available analytical models for the thermal analysis of ground source heat pumps (GSHPs) either neglect groundwater flow or axial effects. In the present study a new analytical approach which considers both effects is developed. Comparison with existing analytical solutions based on the finite and infinite line source theory is carried out. This study shows that in general the heat transfer at the borehole heat exchanger (BHE) is affected by groundwater flow and axial effects. The latter is even more important for long simulation times and short borehole lengths. At the borehole wall the influence of the axial effect is restricted to Peclet numbers lower than 10, assuming the BHE length as characteristic length. Moreover, the influence of groundwater flow is negligible for Peclet numbers lower than 1.2. As a result for Peclet numbers between 1.2 and 10 the combined effect of groundwater flow and axial effects has to be accounted for when evaluating the temperature response of a BHE at the borehole wall and thus the use of the moving finite line source model is required.

[2] Molina-Giraldo, N., P. Blum, K. Zhu, P. Bayer, and Z. Fang. 2011. *Int. J. Therm. Sci*. doi:10.1016/j.ijthermalsci.2011.06.012.

4.1. Introduction

Ground source heat pump (GSHP) systems are one of the major technologies for shallow geothermal energy production in many countries (Lund et al. 2005; Hähnlein et al. 2010b). Through their use, significant amounts of fossil fuels can be saved and thus additional CO_2 emissions can be avoided (Blum et al. 2010; Saner et al. 2010). GSHP systems are closed systems, in which a heat carrier fluid is circulated within a buried vertical or horizontal borehole heat exchanger (BHE). By slow and permanent circulation, exchange of heat with the surrounding underground is accomplished, which is utilized for space heating, air conditioning and hot water supply of both commercial and residential buildings. Vertical borehole configurations are often favored to horizontal collectors because of their smaller space requirements and because they are less influenced by seasonal temperature fluctuations from the surface. In this system, one or more vertical pipes are installed down to depths of around 50 to 150 m (Mustafa Omer 2008), depending on the prevailing geological conditions and the specific energy demand.

In order to estimate the heat transfer at the vertical BHE, different numerical (Chiasson et al. 2000; De Carli et al. 2010; Kim et al. 2010; Lazzari et al. 2010; Lee and Lam 2008; Fan et al. 2007) and analytical methods (Bandos et al. 2009; Carslaw and Jaeger 1959; Diao et al. 2004; Eskilson 1987; Man et al. 2010; Sutton et al. 2003; Zeng et al. 2002; Michopoulos and Kyriakis 2009; Yang et al. 2009; Hähnlein et al. 2010a) as well as combination of the latter have been proposed (Eskilson 1987; Hellström 1991; Yavuzturk 1999). Analytical solutions are widely used because of their simplicity and speed in computation. Most of the analytical approaches for the thermal analysis of BHEs presume conduction-dominated systems (i.e. natural groundwater flow is not considered), and they are based on the infinite line source or cylindrical source theory (Carslaw and Jaeger 1959; Eskilson 1987). They are in particular applied for the evaluation of short-term geothermal field experiments such as thermal response tests (TRT) which usually range from 12 to 60 hours (Signorelli et al. 2007). These models, however, are less adequate for long-term simulations when axial effects become relevant, usually after 1.6 year of operation depending on the hydrogeological and operational conditions (Philippe et al.

2009). The temperature response for an infinite line source model (without groundwater flow) cannot reach steady state conditions and the temperature anomaly will increase to infinity with operation time.

In contrast, the temperature response converges to steady state conditions when accounting for a finite length of the borehole and hence axial effects are considered. Axial effects can be quantified as the differences between the results obtained by using finite and infinite line source methods. The axial heat conduction at the bottom of the borehole accelerates the heat exchange between heat carrier fluid and the surrounding underground, and thus has to be regarded for optimal borehole design. For a specific energy demand of a GSHP system, accounting for the axial effects can reduce the required length and numbers of boreholes. Marcotte et al. (2010) showed for an example design problem that the calculated borehole length could be 15% shorter when axial effects are considered, which ultimately means a more cost-efficient system. Since under many circumstances the axial effects are of high relevance, apposite analytical solutions have been developed. Eskilson (1987) proposed the finite line source model by summing up the effect of point sources of equal energy injection/extraction. This model was improved and used for the evaluation of long-term behavior of BHEs (Lamarche and Beauchamp 2007; Zeng et al. 2002; Marcotte and Pasquier 2008). These analytical solutions account for the axial effects; however, they do not consider groundwater flow.

If groundwater flow is present, advective transport has to be considered, which means that heat is also transported by the moving water. Chiasson et al. (2000), Wang et al. (2009), Fan et al. (2007) and Raymond et al. (2011) evaluated the effects of groundwater flow on the heat transfer into the BHE. They concluded that groundwater flow enhances heat transfer between the BHE and the aquifer. In this case, shorter or less BHEs are needed for the same technical performance. Sutton et al. (2003) and Diao et al. (2004) presented an analytical solution considering groundwater advection. They both concluded that groundwater flow can change considerably the temperature distribution in the vicinity of the borehole. In these analytical solutions the borehole is considered as an infinite line heat source and therefore the axial effects are not taken into account in either study.

Hence, the aim of the present study is to develop an analytical solution which takes into account both aspects: groundwater flow and axial effects. It overcomes the limitations of previous analytical models especially for long-term simulation. The new analytical approach is verified with the finite element code FEFLOW version 6.0 (DHI-WASY 2010). This commercial software package was already used

in several studies for simulating applications of shallow geothermal energy (e.g., Kupfersberger 2009; Nam et al. 2008). The new analytical formulation is also compared to existing analytical methods in order to discuss the influence of axial effects and groundwater flow on the temperature development at the borehole wall and around the BHE.

4.2. Existing analytical approaches

The presence of groundwater flow in the underground and the influence of the actual length of the borehole are rarely taken into account when simulating heat transfer of GSHP systems. Therefore, conduction dominated systems are usually assumed and the borehole is approximated as an infinite line source. Few studies, however, have incorporated the effect of groundwater flow (moving infinite line source model) (Diao et al. 2004; Sutton et al. 2003) or the axial effect (standard finite line source model) (Eskilson 1987; Zeng et al. 2002) in thermal analysis of BHEs. In the following section, these analytical models are presented.

There are other processes that influence the temperature response of the BHE, and therefore should be accounted for in other analytical solutions. Bandos et al. (2009), for instance, developed finite length analytical solutions including vertical temperature variations caused by geothermal gradient and temperature fluctuations at the surface. Man et al. (2010) proposed a solid cylindrical source model which considers the radial dimension of the BHE. The latter is suitable for short boreholes or piles in which the diameter becomes important in comparison with the installation depth. These approaches, however, are not shown in the present study and the focus of the paper is oriented to the combined effect of groundwater flow and axial effects.

4.2.1. Standard finite line source model – (FLS)

Traditionally, heat transport in porous medium without groundwater flow is described by the heat conduction equation (Carslaw and Jaeger 1959), which can be expressed as follows:

$$\rho_m c_m \frac{\partial T}{\partial t} - \nabla \cdot (\lambda_m \nabla T) = 0 \qquad (4\text{-}1)$$

where T denotes the average temperature of the porous medium in which local thermal equilibrium is assumed (Moyne et al. 2000), λ_m is the bulk thermal conductivity, and $\rho_m c_m$ is the volumetric heat

capacity of the bulk porous medium. The latter can be computed as the weighted arithmetic mean of the solids of the aquifer ($\rho_s c_s$) and water ($\rho_w c_w$) (de Marsily 1986):

$$\rho_m c_m = \theta \rho_w c_w + (1-\theta)\rho_s c_s \tag{4-2}$$

The solution of the partial differential equation of heat transport (equation (4-1)) for a continuous point source in an infinite porous medium with a uniform initial temperature (T_o) is given by (Carslaw and Jaeger 1959):

$$\Delta T(x, y, z, t) = \frac{Q}{4\pi\lambda_m r} erfc\left[\frac{r}{\sqrt{4at}}\right] \tag{4-3}$$

where ΔT is the temperature change in the underground (T_o-T), Q is the heat flow rate extracted/injected, a the thermal diffusivity ($a = \lambda_m/\rho_m c_m$), and $r = \sqrt{x^2 + y^2 + (z-z')^2}$ is the distance to the source located on the z-axis at the coordinates (0, 0, z'). The FLS model is constructed by applying the method of images and summing up contributions of the point sources of equal energy injection/extraction (Lamarche and Beauchamp 2007; Marcotte et al. 2010; Zeng et al. 2002; Eskilson 1987). As a result, constant temperature boundary conditions at the surface and downward vertical heat flow losses (axial effects) are accounted for. Applying the method of images (Eskilson 1987; Zeng et al. 2002) to equation (4-3) yields:

$$\Delta T_{\mathrm{FLS}}(x, y, z, t) = \frac{q_L}{4\pi\lambda_m}\left[\int_0^H \frac{1}{r} erfc\frac{r}{\sqrt{4at}} dz' - \int_{-H}^0 \frac{1}{r} erfc\frac{r}{\sqrt{4at}} dz'\right] \tag{4-4}$$

where H is the borehole length. For steady state conditions, equation (4-4) reduces to:

$$\Delta T_{\mathrm{FLSs}}(x, y, z) = \frac{q_L}{4\pi\lambda_m} \ln\left[\frac{H - z + \sqrt{r'^2 + (H-z)^2}}{H + z + \sqrt{r'^2 + (H+z)^2}} \frac{2z^2 + 2z\sqrt{r'^2 + z^2} + r'^2}{r'^2}\right] \tag{4-5}$$

where $r' = \sqrt{x^2 + y^2}$. Introducing the dimensionless temperature rise $\Theta = 4\pi\lambda_m \Delta T / q_L$, the dimensionless coordinates $R' = \sqrt{x^2 + y^2}/H$, $R = \sqrt{R'^2 + (Z - Z')^2}$, $Z = z/H$, and $Z' = z'/H$, and the Fourier number $Fo = at/H^2$, we can express equations (4-4) and (4-5) in dimensionless forms:

$$\Theta_{\mathrm{FLS}}(R',Z,Fo)=\left[\int_{0}^{1}\frac{1}{R}erfc\frac{R}{2\sqrt{Fo}}dZ'-\int_{-1}^{0}\frac{1}{R}erfc\frac{R}{2\sqrt{Fo}}dZ'\right] \tag{4-6}$$

$$\Theta_{\mathrm{FLSs}}(R',Z)=\ln\left[\frac{1-Z+\sqrt{R'^2+(1-Z)^2}}{1+Z+\sqrt{R'^2+(1+Z)^2}}\frac{2Z^2+2Z\sqrt{R'^2+Z^2}+R'^2}{R'^2}\right] \tag{4-7}$$

4.2.2. Moving infinite line source model – (MILS)

Heat transport in the porous media with groundwater flow is mainly accomplished by conduction through the fluid and solid phase and advection through the flowing water. The partial differential equation for advective and conductive heat transport in porous media can be expressed in a 2D form (*x*-*y* plane) as follows (Domenico and Schwartz 1998):

$$\rho_m c_m\frac{\partial T}{\partial t}+q\rho_w c_w\frac{\partial T}{\partial x}-\lambda_m\left(\frac{\partial^2 T}{\partial x^2}+\frac{\partial^2 T}{\partial y^2}\right)=0 \tag{4-8}$$

where q denotes an uniform Darcy velocity in the x-direction. The solution of equation (4-8) for an infinite porous medium with a uniform initial temperature is given by Sutton et al. (2003) and Diao et al. (2004):

$$\Delta T_{\mathrm{MILS}}(x,y,t)=\frac{q_L}{4\pi\lambda_m}\exp\left[\frac{v_{\mathrm{T}}x}{2a}\right]\int_{0}^{v_T^2t/4a}\frac{1}{\psi}\exp\left[-\psi-\frac{v_{\mathrm{T}}^2(x^2+y^2)}{16a^2\psi}\right]d\psi \tag{4-9}$$

in which $v_{\mathrm{T}}=q\rho_w c_w/\rho_m c_m$ is the effective heat transport velocity. This analytical solution applies for the response of a constant line source with infinite length along the *z*-direction with a continuous heat flow rate per unit length of the borehole, q_L. Although a BHE is composed of a buried pipe that commonly is surrounded by grouting material, approximation by a line source is commonly accepted in heat transport models of GSHP systems (Diao et al. 2004; Eskilson 1987; Sutton et al. 2003). The underground is assumed to be homogeneous with respect to the thermal and hydraulic parameters. For steady state conditions equation (4-9) becomes:

$$\Delta T_{\mathrm{MILSs}}(x,y)=\frac{q_L}{2\pi\lambda_m}\exp\left[\frac{v_{\mathrm{T}}x}{2a}\right]K_0\left[\frac{v_{\mathrm{T}}\sqrt{x^2+y^2}}{2a}\right] \tag{4-10}$$

in which K_0 is the modified Bessel function of the second kind of order zero. Introducing the dimensionless variable $Pe = v_T H / a$ (Peclet number), we can express equations (4-9) and (4-10) in dimensionless forms as follows:

$$\Theta_{\mathrm{MILS}}(R', \varphi, Fo, Pe) = \exp\left[\frac{Pe}{2} R' \cos(\varphi)\right] \int_0^{Pe^2 Fo/4} \frac{1}{\psi} \exp\left[-\psi - \frac{Pe^2 R'^2}{16\psi}\right] d\psi \tag{4-11}$$

$$\Theta_{\mathrm{MILSs}}(R', \varphi, Pe) = 2 \exp\left[\frac{Pe}{2} R' \cos(\varphi)\right] K_0\left[\frac{Pe}{2} R'\right] \tag{4-12}$$

Groundwater flow velocities are highly variable depending on the hydrogeological conditions. This variability is especially attributed to the hydraulic conductivity which can range over more than 8 orders of magnitude (Spitz and Moreno 1996). For instance, the hydraulic conductivity of sandy sediments can vary from 10^{-5} to 10^{-3} m/s. Assuming a constant and typical hydraulic gradient of 10^{-3}, the Darcy velocity ranges from 10^{-8} to 10^{-6} m/s for fine and coarse sands, respectively.

4.3. Moving finite line source model – (MFLS). New approach

For long-term period simulations, axial effects become more evident when simulating heat transfer at the BHE (Marcotte et al. 2010). Existing analytical solutions that account for axial effects still do not consider groundwater flow. Hence, the new analytical approach proposed here takes into account both effects, while the following assumptions are made:

a) The underground is considered as a homogeneous semi-infinite porous medium, which is initially at thermal equilibrium and its thermal properties are independent of the temperature changes.

b) The boundary of the ground surface has a fixed temperature equal to the initial temperature of the underground and natural geothermal gradient is not accounted for.

c) A constant heat flow rate per unit length of the borehole (q_L) is applied to a line source of finite length, which stretches along the *z*-axis down to a certain depth *H*.

The starting point for the finite line source model is the Green's function of an instantaneous point source (equation (B-1)). The moving finite line source model is obtained by applying the method of

images (Eskilson 1987) and the moving source theory (Carslaw and Jaeger 1959) to equation (B-1). The detailed derivation is presented in the Appendix B.

The transient solution reads:

$$\Delta T_{\mathrm{MFLS}}(x,y,z,t)=\frac{q_L}{2\pi\lambda_m}\exp\left[\frac{v_T x}{2a}\right]\left[\int_0^H f(x,y,z,t)dz'-\int_{-H}^0 f(x,y,z,t)dz'\right] \tag{4-13}$$

$$f(x,y,z,t)=\frac{1}{4r}\left[\exp\left(-\frac{v_T r}{2a}\right)erfc\left(\frac{r-v_T t}{2\sqrt{at}}\right)+\exp\left(\frac{v_T r}{2a}\right)erfc\left(\frac{r+v_T t}{2\sqrt{at}}\right)\right] \tag{4-14}$$

As time approaches infinity, the steady state solution is derived as follows:

$$\Delta T_{\mathrm{MFLSs}}(x,y,z)=\frac{q_L}{4\pi\lambda_m}\exp\left[\frac{v_T x}{2a}\right]\left[\int_0^H \frac{1}{r}\exp\left[-\frac{v_T r}{2a}\right]dz'-\int_{-H}^0 \frac{1}{r}\exp\left[-\frac{v_T r}{2a}\right]dz'\right] \tag{4-15}$$

In order to keep the number of independent variables to the minimum, equations (4-13)-(4-15) can be expressed in dimensionless forms:

$$\Theta_{\mathrm{MFLS}}(R',Z,\varphi,Fo,Pe)=2\exp\left[\frac{Pe}{2}R'\cos(\varphi)\right]\left[\int_0^1 f(R,Fo,Pe)dZ'-\int_{-1}^0 f(R,Fo,Pe)dZ'\right] \tag{4-16}$$

$$f(R',Z,Fo,Pe)=\frac{1}{4R}\left[\exp\left(-\frac{Pe}{2}R\right)erfc\left(\frac{R-PeFo}{2\sqrt{Fo}}\right)+\exp\left(\frac{Pe}{2}R\right)erfc\left(\frac{R+PeFo}{2\sqrt{Fo}}\right)\right] \tag{4-17}$$

$$\Theta_{\mathrm{MFLSs}}(R',Z,\varphi,Pe)=\exp\left[\frac{Pe}{2}R'\cos(\varphi)\right]\left[\int_0^1 \frac{1}{R}\exp\left[-\frac{Pe}{2}R\right]dZ'-\int_{-1}^0 \frac{1}{R}\exp\left[-\frac{Pe}{2}R\right]dZ'\right] \tag{4-18}$$

4.4. Results and discussion

4.4.1. Validation of the new moving finite line source model

In order to validate the new analytical approach, a comparison with a numerical simulation is needed. In the present work, the finite element code FEFLOW version 6.0 (DHI-WASY 2010) is used to solve the same heat transport problem. A three-dimensional (3D) model is constructed with a horizontal domain size of 100 m × 200 m (Figure 4-1) and with 20 identical 5 m layers (100 m depth). The BHE

is represented by a line source for the first 50 m (top 10 layers) with an average heat flow rate of 20 W/m during 20 years of simulation. A thickness of 50 m is assigned below the BHE in order to minimize boundary effects by the model bottom while still including axial effects. Fixed-head boundary conditions are applied to the left and the right model boundaries. Uniform groundwater flow is assigned throughout the aquifer. Thermal parameters of the aquifer are selected as follows: λ_m = 2.5 W/m/K, θ = 0.26, c_s = 880 J/kg/K and ρ_s = 2650 kg/m^3. The hydraulic and thermal parameters are assumed to be independent of the temperature changes. Hecht-Méndez et al. (2010), for instance, stated that variable density and viscosity due to temperature changes are negligible under typical hydrogeological and operational conditions of GSHP systems.

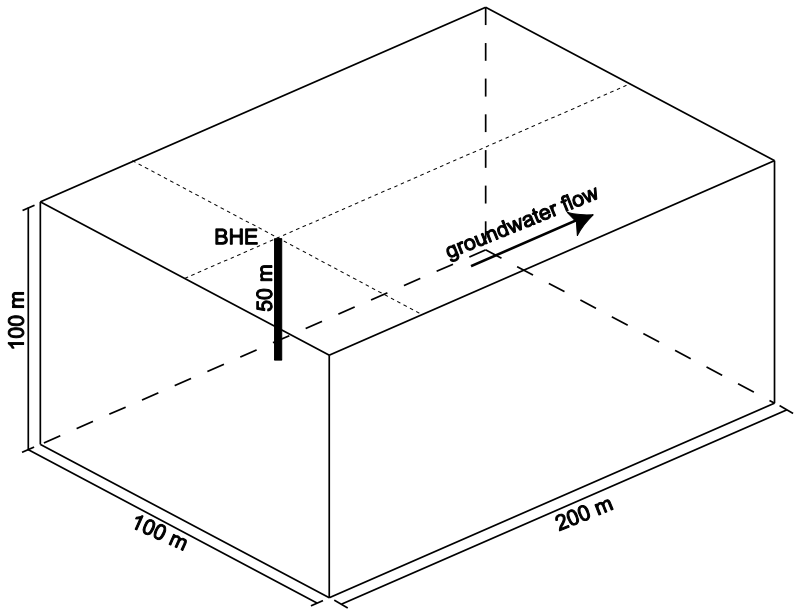

Figure 4-1. 3D model used in the validation. The BHE is represented by a line source in the top 50 m.

Given that temperature changes instead of the absolute temperature are simulated, an initial temperature of 0 °C is assigned to the entire domain. Moreover, fixed ground surface temperature of 0 °C is assigned to the top layer in order to fulfil the requirements of the analytical solution.

The comparison of the analytical results with the numerical code is shown in Figure 4-2. Dimensionless temperature is plotted against dimensionless distance, R', for Pe = 8 and Fo = 0.2 (Figure 4-2a). Moreover, dimensionless temperature is also plotted against the Fourier number for two Peclet numbers, Pe = 4 and Pe = 8 (Figure 4-2b). It can be seen in both figures that the temperature response of the analytical solution agrees with the numerical solution. Calculation of the root mean squared error

yields values of 0.02 for Figure 4-2a, and 0.03 for Figure 4-2b. It has to be mentioned that other Peclet number scenarios as well as different space locations (*x*, *y*, *z*) were evaluated and also produced satisfactory results with the comparisons.

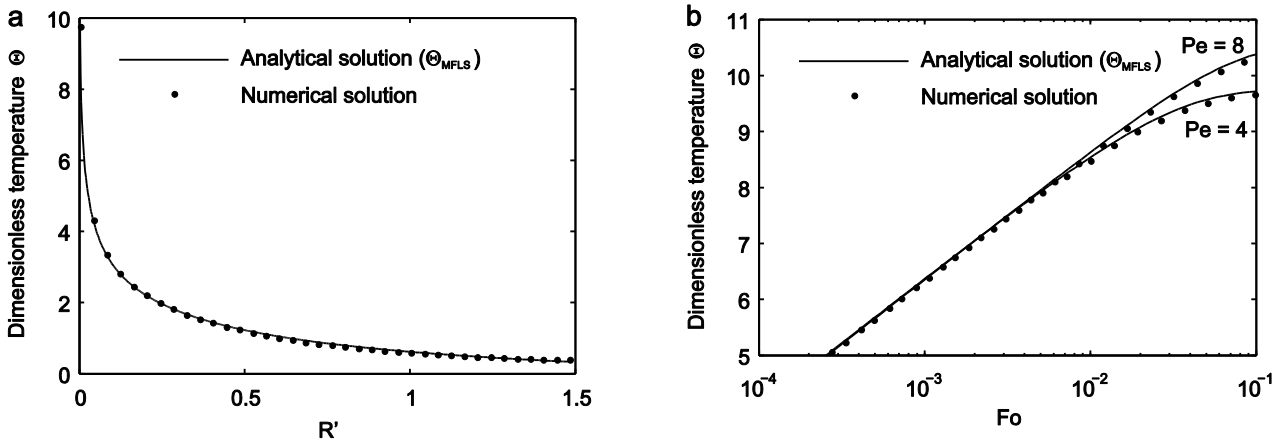

Figure 4-2. Comparison of analytical (equation (4-16)) and numerical results (y = 0 m, z = 0.5H, H = 50 m): (a) temperature response (dimensionless temperature, $\Theta = 4\pi\lambda_m \Delta T / q_L$) over dimensionless distance $R' = x / H$ (Fo = 0.2, Pe = 8); (b) temperature response over Fourier number, $Fo = at / H^2$ (R' = 0.002).

4.4.2. Influence of axial effects and groundwater flow on the temperature response

In order to assess the scope of the new moving finite line source model (Θ_{MFLS}), a comparison with the standard finite line source model (Θ_{FLS}) and the moving infinite line source model (Θ_{MILS}) is carried out. Note that the thermal parameters of the aquifer are set equal to the ones used in section 4.4.1. Figure 4-3 depicts relative temperature contours (isotherms) obtained by the MFLS and MILS models in which groundwater advection is considered. Relative temperature means that the isotherms delineate a temperature difference, ΔT, between the temperature plume and ambient conditions. Note that temperature plumes are shorter for the MFLS model (Figure 4-3a). Axial effects yield lower temperature changes at any given distance from the source due to the vertically dissipated heat. Therefore, neglecting axial effects could result in over-sizing of the calculated borehole lengths in designing problems for a certain energy demand (Marcotte et al. 2010). Figure 4-3b reveals the temperature anomaly created in the vertical direction due to the axial effects. Obviously the differences between the models are most evident close to the end points of the borehole.

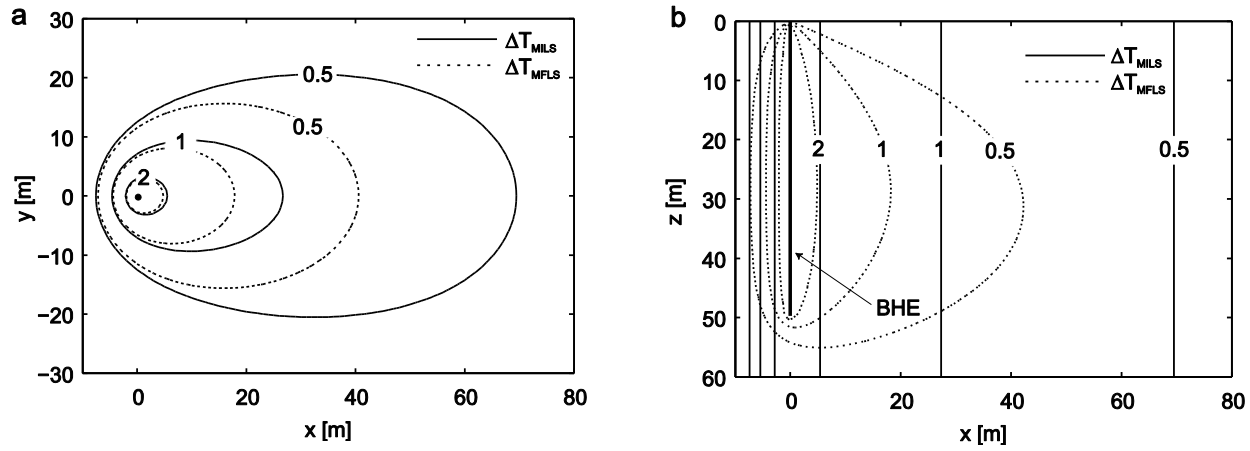

Figure 4-3. Temperature change isotherms contours, ΔT [K]. Dashed lines: MFLS model with H = 50 m (equation (4-13)); solid lines: MILS model (equation (4-9)). (a) Plan view (z = 0.5H); (b) vertical cross section along centerline (y = 0 m). (q_L = 20 W/m, Fo = 0.2, Pe = 8).

Figure 4-4 shows the temperature response of the MILS model (continuous black line) and the MFLS model (intermittent black lines) over a dimensionless time (Fo / R'^2) for different borehole lengths. The figure clearly shows the effect of the simulation time and the borehole length on the discrepancy between the MFLS and MILS models. For longer times the discrepancy becomes more evident. Furthermore, the shorter the borehole length becomes, the earlier the time when the MFLS and MILS models start to differ and the more dominant the difference between both models. Note that the dimensionless temperature is evaluated at the center of the borehole (z = H/2), which is a common choice to approximate the temperature at the borehole wall. For steady state conditions, however, an overestimation of the temperature can occur (Lamarche and Beauchamp 2007; Zeng et al. 2002). Therefore, the mean temperature along the borehole length is discussed as better option for steady state conditions (Lamarche and Beauchamp 2007; Philippe et al. 2009; Zeng et al. 2002). In the present study, for the sake of simplicity the former option is chosen.

The influence of the length of the borehole can also be seen in Figure 4-5, where the temperature response is plotted over borehole lengths varying from 0 to 200 m. The shorter the borehole length is, the larger the discrepancy between the MFLS and MILS models is. For instance, for the conditions given in Figure 4-5 with a Darcy velocity of 1×10^{-7} m/s, the models start to differ after around 2 years for boreholes with lengths shorter than 50 m. Moreover, for steady state conditions, the MILS model is valid only for a borehole length longer than 100 m.

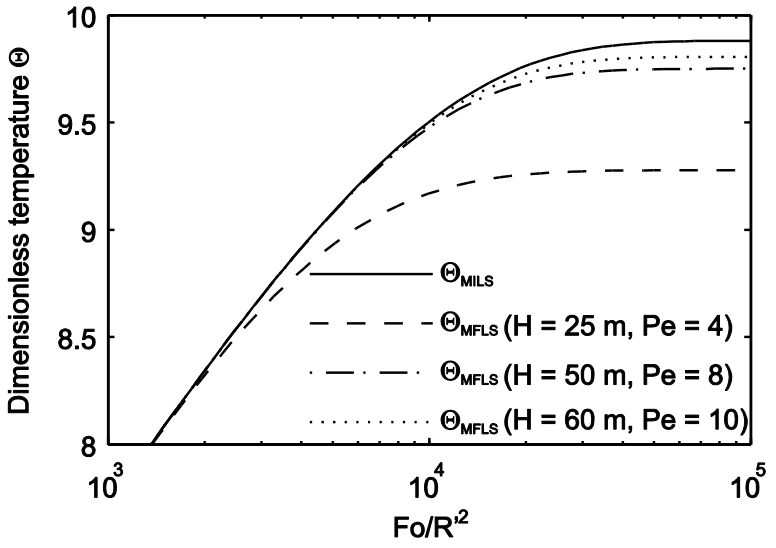

Figure 4-4. Temperature response over dimensionless number $Fo/R'^2 = at/x^2$ for different borehole lengths (q = 1 × 10^{-7} m/s, x = 0.1 m, y = 0 m, z = 0.5H). Θ_{MILS}: moving infinite line source model (equation (4-11)); Θ_{MFLS}: moving finite line source model (equation (4-16)).

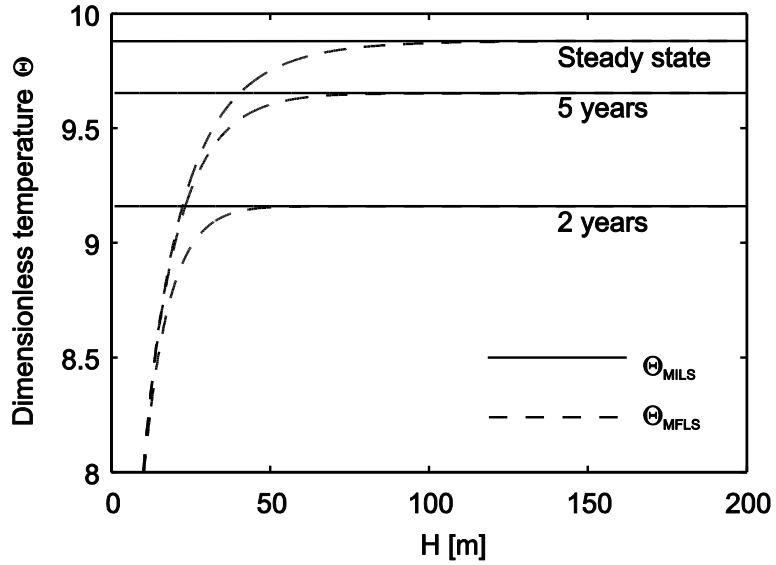

Figure 4-5. Temperature response over borehole length H. (q = 1 × 10^{-7} m/s, x = 0.1m, y = 0 m, z = 0.5H, Pe = 0 for H = 0 m and Pe = 33 for H = 200 m). Θ_{MILS}: moving infinite line source model (equation (4-11) and (4-12)); Θ_{MFLS}: moving finite line source model (equation (4-16) and (4-18)).

In order to assess both the influence of groundwater flow and the axial effect, the mean temperature around a circle is evaluated for equations (4-6), (4-11) and (4-16). Figure 4-3a shows that the temperature isotherms are not symmetrical with respect to the polar angle. Therefore, the mean

temperature around a circle for the moving finite (equation (4-16)) and infinite line (equation (4-11)) source models can be defined as the integral average of a circle of given radius (Diao et al. 2004):

$$\Theta_{\mathrm{MILSm}}(R', Fo, Pe) = \frac{1}{\pi}\int_0^{\pi} \Theta_{\mathrm{MILS}}(R', \varphi, Fo, Pe) d\varphi \tag{4-19}$$

$$\Theta_{\mathrm{MFLSm}}(R', Z, Fo, Pe) = \frac{1}{\pi}\int_0^{\pi} \Theta_{\mathrm{MFLS}}(R', Z, \varphi, Fo, Pe) d\varphi \tag{4-20}$$

The ratios $\Theta_{\mathrm{MFLSm}}/\Theta_{\mathrm{MILSm}}$ and $\Theta_{\mathrm{MFLSm}}/\Theta_{\mathrm{FLS}}$ as functions of the Fourier number for different Peclet numbers are shown in Figure 4-6. A decrease in these values represents an increase in the discrepancy between the MFLS and MILS model (Figure 4-6a) and therefore indicates a major influence of the axial effects. Similarly, in Figure 4-6b it can be seen that a decrease in the ratio corresponds to a larger discrepancy between the MFLS and FLS model (Figure 4-6b) and therefore, there is a major influence of the groundwater flow.

Figure 4-6a indicates that the temperature reaches the steady state condition faster at higher groundwater flow velocities. In addition, for long term simulations, the discrepancy between the models increases. This figure also reflects the effect of groundwater flow on the axial effects. It is noticeable that the larger the Peclet number the smaller the difference between the MFLS and MILS model. Hence, the axial effects are more important for low groundwater velocities. For Peclet numbers larger than 10, the discrepancy between the moving finite and the infinite solutions becomes irrelevant ($\Theta_{\mathrm{MFLSm}}/\Theta_{\mathrm{MILSm}} > 0.99$) at the borehole wall ($x$ = 0.1 m). In the specific case of a borehole length of 50 m, the axial effects are negligible for Darcy velocities larger than 1.2×10^{-7} m/s (assuming λ_m = 2.5 W/m/K). Therefore, the MILS model is still valid even for long term simulations in this groundwater flow scenario.

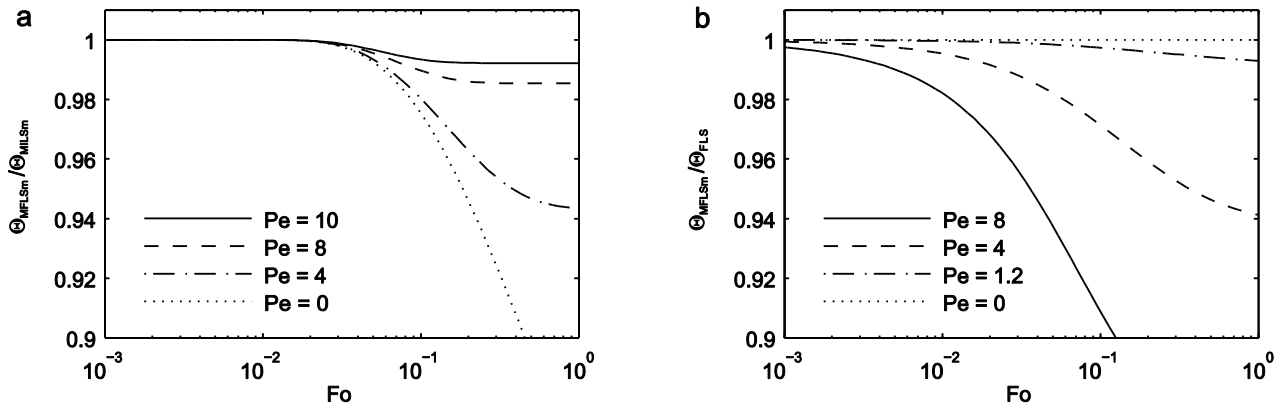

Figure 4-6. Temperature response of a circle around the heat source (r = 0.1 m, H = 50 m, z = 0.5H m): (a) ratio of the MFLS and MILS model; (b) ratio of the MFLS and FLS model.

On the other hand, Figure 4-6b shows that the discrepancy between the standard finite and moving finite line source model becomes irrelevant ($\Theta_{MFLSm}/\Theta_{FLS} > 0.99$) at the borehole wall ($x$ = 0.1 m) for Peclet numbers lower than 1.2. Therefore, the influence of groundwater flow can be neglected in these Peclet numbers scenarios. From the aforementioned discussion, it is clear that both effects combined, axial and groundwater flow, have a major influence on the thermal response of a BHE for Peclet numbers between 1.2 and 10. It has to be mentioned that the presented results are expressed based on a Peclet number, in which the characteristic length is set to be the borehole length (H). This is to emphasize that this parameter determines the finite length of a BHE, the focus of this work. The Peclet number is a common indicator to compare the role of convection to that of conduction, but as in our study the characteristic length is defined dependent on the scale of investigation. For instance, it is set the borehole spacing (Chiasson et al. 2000), the borehole radius (Sutton et al. 2003), and the radial distance (Diao et al. 2004). Chiasson et al. (2000) stated that advection has a significant effect on the GSHP system performance for $Pe > 1$. Sutton et al. (2003) showed that for $Pe > 0.01$, the ground temperature response when advection is considered highly differs from the response with only conduction. Finally, Diao et al. (2004) revealed that for Pe > 0.005 the impact of groundwater flow must be accounted for. Due to the different underlying characteristics lengths, these values, however, are not directly comparable. For the specific case of H = 50 m, when normalizing our results with respect to the aforementioned characteristic lengths, we obtain equivalent Pe = 0.11, 0.0013 and 0.002 for Chiasson et al. (2000), Sutton et al. (2003), and Diao et al. (2004), respectively. These values are lower than ones suggested by the previous studies. However, this reflects the effect of accounting for a finite length and the criteria employed to decide whether advection or conduction is more relevant

($\Theta_{MFLSm}/\Theta_{FLS} > 0.99$). Additionally, our results reveal the effect of groundwater flow when axial effects are accounted for.

4.5. Conclusions

We presented a new analytical approach for the finite line source model that accounts for groundwater flow. The expression is derived for 3D and accounts for a constant surface temperature and vertical heat losses (axial effects). The influence of axial effects and groundwater flow on the temperature response of a BHE is assessed by comparing the new approach (moving finite line source model - MFLS) with existing analytical solutions such as the standard finite line source (FLS) model and moving infinite line source (MILS) model. Moreover, the new approach is also validated with a numerical code.

In general, we can conclude that both the groundwater flow and the axial heat flow have an effect on the temperature response from a borehole heat exchanger. Losses of heat downwards from the borehole bottom and fix temperature conditions at the surface result in lower temperature changes in the underground surrounding the BHE. This effect becomes more evident and therefore the discrepancy between the MFLS and MILS model increases with longer simulation time and shorter borehole lengths.

These axial effects, however, have a minor impact on the temperature response for high groundwater flow scenarios. Therefore, the discrepancy between the MFLS and MILS model decreases when increasing velocity. At the borehole wall (x = 0.1 m), axial effects can be neglected for Peclet numbers larger than 10. On the other hand, for low groundwater flow scenarios (Pe < 1.2) the effect of groundwater flow is negligible and only the axial effects play an important role.

We can conclude that the role of axial effects mainly depends on the groundwater velocity in the aquifer and the length of the borehole heat exchanger. The new proposed analytical approach (MFLS) can be applied to all groundwater flow conditions and borehole lengths. However, for $Pe < 1.2$ the use of the FLS model is still valid and for $Pe > 10$ the use of the MILS approach is acceptable. For a Peclet number range between 1.2 and 10 the use of the MFLS model is required. As an example, the temperature response of a borehole of 50 m in an aquifer with Darcy velocities of 1×10^{-8} m/s (Pe = 0.8) and 1×10^{-6} m/s (Pe = 84) can still be well represented by the FLS model and the MILS model,

respectively. For an intermediate Darcy velocity of 1×10^{-7} m/s (Pe = 8.4), the temperature response however must be evaluated by the MFLS model.

Future work will be dedicated to evaluate the combined effect of groundwater flow, axial effects and natural geothermal gradient together with variable heat load and multiple boreholes.

Appendix B

MFLS derivation

An instantaneous energy extracted/injected (Q_1) at a point located at (x',y',z') produces a temperature increment given by the following Green's function (Carslaw and Jaeger 1959) which satisfies the partial differential equation given by equation (4-1):

$$\Delta T(x,y,z,t) = \frac{Q'}{8\rho c(\pi a t)^{3/2}} \exp\left[-\frac{(x-x')^2+(y-y')^2+(z-z')^2}{4at}\right] \qquad \text{(B-1)}$$

The temperature response at a given time t due to a energy extracted/injected $Qd\tau$ for a continuous point source after applying the moving source theory (Carslaw and Jaeger 1959) yields the moving point source equation for a continuous injection:

$$\Delta T(x,y,z,t) = \frac{Q}{8\rho c(\pi a)^{3/2}} \int_0^t \frac{1}{(t-\tau)^{3/2}} \exp\left[-\frac{[x-v_T(t-\tau)]^2+(y-y')^2+(z-z')^2}{4a(t-\tau)}\right] d\tau \qquad \text{(B-2)}$$

Applying a change of variable, $\psi = r^2/4a(t-\tau)$, we obtain:

$$\Delta T(x,y,z,t) = \frac{Q}{2\pi^{3/2}\lambda_m r} \exp\left[\frac{v_T x}{2a}\right] \int_{r/2\sqrt{at}}^{\infty} \exp\left[-\psi^2 - \frac{v_T^2 r^2}{16a^2\psi^2}\right] d\psi \qquad \text{(B-3)}$$

For steady state conditions equation (B-3) becomes:

$$\Delta T(x,y,z) = \frac{Q}{4\pi\lambda_m r} \exp\left[-\frac{v_T(r-x)}{2a}\right] \qquad \text{(B-4)}$$

In order to account for axial effects and constant ground surface temperature conditions, the method of images (Carslaw and Jaeger 1959; Eskilson 1987) is applied to equation (B-3):

$$\Delta T_3(x,y,z,t) = \frac{q_L}{2\pi\lambda}\exp\left[\frac{v_T x}{2a}\right]\left[\int_0^H f(x,y,z,t)dz' - \int_{-H}^0 f(x,y,z,t)dz'\right] \quad \text{(B-5)}$$

where:

$$f(x,y,z,t) = \frac{1}{r\sqrt{\pi}}\int_{r/2\sqrt{at}}^{\infty}\exp\left[-\psi^2 - \frac{v_T^2 r^2}{16a^2\psi^2}\right]d\psi \quad \text{(B-6)}$$

Equation (B-5) is too complex to solve, therefore a change of variable ($u = \psi^2$) is applied in order to simplify equation (B-6) as follows:

$$f(x,y,z,t) = \frac{1}{2r\sqrt{\pi}}\int_{r^2/4at}^{\infty}\frac{1}{\sqrt{u}}\exp\left[-u - \frac{v_T^2 r^2}{16a^2 u}\right]du \quad \text{(B-7)}$$

The integral of equation (B-7) can be expressed as the generalized incomplete gamma function (Chaudhry and Zubair 1994):

$$f(x,y,z,t) = \frac{1}{2r\sqrt{\pi}}\Gamma\left(\frac{1}{2}, \frac{r^2}{4at}; \frac{v_T^2 r^2}{16a^2}\right) \quad \text{(B-8)}$$

Moreover, the generalized incomplete gamma function can be expressed as a function of exponential and complementary error functions as follows (Chaudhry and Zubair 1994):

$$\Gamma\left(\frac{1}{2}, u_1; u_2\right) = \frac{1}{2}\sqrt{\pi}\left[\exp\left(-2\sqrt{u_2}\right)erfc\left(\sqrt{u_1} - \frac{\sqrt{u_2}}{\sqrt{u_1}}\right) + \exp\left(2\sqrt{u_2}\right)erfc\left(\sqrt{u_1} + \frac{\sqrt{u_2}}{\sqrt{u_1}}\right)\right] \quad \text{(B-9)}$$

Therefore, equation (B-7) reduces to:

$$f(x,y,z,t) = \frac{1}{4r}\left[\exp\left(-\frac{v_T r}{2a}\right)erfc\left(\frac{r - v_T t}{2\sqrt{at}}\right) + \exp\left(\frac{v_T r}{2a}\right)erfc\left(\frac{r + v_T t}{2\sqrt{at}}\right)\right] \quad \text{(B-10)}$$

For steady state conditions, the method of images applied to equation (B-4) yields:

$$\Delta T_3(x,y,z) = \frac{q_L}{4\pi\lambda_m}\exp\left[\frac{v_T x}{2a}\right]\left[\int_0^H \frac{1}{r}\exp\left[-\frac{v_T r}{2a}\right]dz' - \int_{-H}^0 \frac{1}{r}\exp\left[-\frac{v_T r}{2a}\right]dz'\right] \quad \text{(B-11)}$$

5. Paper III:

Evaluating the influence of thermal dispersion on temperature plumes from geothermal systems using analytical solutions[3]

Abstract: An analytical study is carried out to examine the effect of thermal dispersion on the simulation of temperature plumes in aquifers that evolve from vertical ground source heat pump (GSHP) systems. Analytical solutions for the simulation of heat transport in aquifers often ignore thermal dispersion. In this study an existing two-dimensional analytical approach for transient conditions is used. Moreover, an equation to calculate the length of the temperature plume for steady state conditions is developed. To study the interplay between thermal dispersion and hydraulic conductivity, Darcy velocities are varied from 10^{-8} m/s to 10^{-5} m/s and thermal dispersivities are varied based on two assumptions: 1) thermal dispersion is assumed to be only dependent on the Darcy velocity and 2) thermal dispersion is assumed to be scale-dependent. The results are discussed with respect to their implications for typical legal regulations and operation of such GSHP systems. In general, the effect of thermal dispersion on the temperature plume around the borehole heat exchanger (BHE) is minor when thermal dispersion is assumed to be depending solely on the magnitude of groundwater flow (e.g., in a homogeneous aquifer). On the other hand, based on a field scale of 10 m and assuming thermal dispersion to be scale-dependent, thermal dispersion can be neglected only for conditions typical for fine sands, clays, and silts with $q < 10^{-8}$ m/s. For aquifers where medium sands and gravels (with Darcy velocities $q > 10^{-8}$ m/s) dominate, thermal dispersion has a larger effect on the temperature plume distribution around the borehole heat exchanger.

[3] Molina-Giraldo, N., P. Bayer, and P. Blum. 2011. *Int. J. Therm. Sci*. 50 no. 7: 1223–1231.

5.1. Introduction

The use of shallow geothermal energy is continuously increasing (Lund et al. 2005) and in particular the application of vertical ground source heat pump (GSHP) systems (Sanner et al. 2003). This technology relies on a simple concept: One or more vertical pipes are installed down to depths of around 50 m – 150 m (Mustafa Omer 2008). The pipes act as borehole heat exchangers (BHEs) that are connected to an aboveground heat pump. Heat exchange is accomplished by circulation of a heat carrier fluid within this closed system. The energy from underground is mostly used for space heating and warm water supply. Alternatively, during warm seasons or when superfluous heat is available, energy can also be injected for storage or to support air-conditioning systems. Geothermal energy is counted among the renewable resources. It offers environmental benefits, since considerable amounts of fossil fuel can be saved and thus additional CO_2 emissions can be avoided or even reduced (Blum et al. 2010; Saner et al. 2010).

The use of GSHP systems yields temperature plumes in the subsurface, which can extend to a significant size and prevail for a long time depending on the hydrogeological conditions and mode of the system, heating or cooling (Hecht-Méndez et al. 2010; Hähnlein et al. 2010a; Pannike et al. 2006). The length of the temperature plume is defined as the distance downgradient from the injection/extraction point to the isotherm contour of interest. Temperature plumes that adversely affect adjacent and neighboring geothermal systems have to be avoided. Thus, they have to be well predicted and controlled to guarantee long-term sustainable use. In some countries, minimum distances between two BHEs and maximum temperature changes allowed in the underground are required. For instance, in the German state of Baden-Württemberg, a distance of 10 m between individual BHEs is suggested by the regulators (Hähnlein et al. 2010a; Hähnlein et al. 2010b). In Switzerland, a distance of 4 m – 8 m is typically recommended between individual BHEs.

Numerical models are widely applied to simulate heat transport in aquifers under the influence of GSHP systems (Chiasson et al. 2000; Fan et al. 2008; Hidalgo et al. 2009). Chiasson et al. (2000) and Fan et al. (2008) evaluated the effects of groundwater flow on the heat transfer into the BHE of GSHP

systems. They concluded that groundwater flow enhances heat transfer between the BHE and the aquifer. Hidalgo et al. (2009) carried out steady state numerical simulations for temperature plumes of BHEs. The principal aim was to find out the influence of hydraulic conductivity heterogeneity on heat transport and thus evaluate the effect of thermal dispersion. Such numerical models are in particular suitable for complex configurations and boundary conditions.

Analytical models are fast and straightforward means to calculate the expected extension of temperature plume, as long as simple configurations are studied and homogeneous aquifers can be assumed. Some analytical approaches to simulate heat transport in the subsurface presume conduction-dominated systems (Carslaw and Jaeger 1959). Heat is transported by thermal diffusion along a temperature gradient and thus the role of groundwater flow (advection) is not taken into account. These types of analytical solutions are based on the line-source theory and are widely used for the evaluation of geothermal applications such as BHE and thermal response tests (Signorelli et al. 2007).

However, if groundwater velocity is present, advective transport has to be considered. Then heat is transported by the moving water, and differential advection occurs due to the different flow pathways that are possible in porous media. This process is called thermal dispersion, and is generated by microscale mixing of the pore-scale interstitial water (Bear 1972; Green et al. 1964) as well as by differential transport in macroscale geological heterogeneities (de Marsily 1986; Ferguson 2007; Hidalgo et al. 2009; Sauty et al. 1982a). Usually, the dominant process is thermal diffusion (Bear 1972).

Analytical approaches are available that model the effect of groundwater flow for an infinite line-source (Sutton et al. 2003; Diao et al. 2004; Carslaw and Jaeger 1959). However, these do not consider thermal dispersion. Even if thermal diffusion is dominant, the error introduced from this simplification is rarely discussed. Depending on the nature of the aquifer, mechanical mixing of heat due to differential convection at the microscopic scale and heterogeneities of the conductivity field can affect the spreading of the heat plume in the subsurface (Nield and Bejan 2006; Ferguson 2007; Hidalgo et al. 2009). Therefore, an evaluation of the importance of considering thermal dispersion in the regulation and monitoring of GSHP systems is required.

In this study an existing two-dimensional (2D) analytical approach for transient conditions which considers thermal dispersion is used. Metzger et al. (2004) developed this analytical solution to

determine thermal dispersion coefficients for a packed bed of glass spheres. This analytical solution, however, has not been applied yet for GSHP systems. In the present study, the latter transient solution is reduced to steady state conditions and an equation to calculate the length of the temperature plume is developed. The principal aim is to analytically characterize the role of thermal dispersion on the simulation of temperature plumes, which develop from GSHP systems in typical natural aquifers. The results are discussed with respect to their implications for the operation of GSHP systems under typical legal regulations such as on the suggested minimum distance between single borehole heat exchangers (BHEs) and neighboring installations.

5.2. Governing equations

5.2.1. Heat transport in the subsurface

Heat transport in porous media is accomplished mainly by conduction through the fluid and solid phase and advection through the moving water. Therefore, it is characterized by the heat advection/dispersion equation, which can be expressed in a 2D form (*x*-*y* plane) as follows (de Marsily 1986):

$$\rho_m c_m \frac{\partial T}{\partial t} + q\rho_w c_w \frac{\partial T}{\partial x} - \lambda_x \frac{\partial^2 T}{\partial x^2} - \lambda_y \frac{\partial^2 T}{\partial y^2} - s = 0 \qquad (5\text{-}1)$$

where T denotes the average temperature of the porous medium in which local thermal equilibrium is assumed (Moyne et al. 2000), q is the uniform Darcy velocity in the x-direction, s is a volumetric heat source, and $\rho_m c_m$ is the volumetric heat capacity of the bulk porous medium. The latter can be computed as the weighted arithmetic mean of the solids of the aquifer ($\rho_s c_s$) and water ($\rho_w c_w$) (de Marsily 1986):

$$\rho_m c_m = \theta \rho_w c_w + (1-\theta)\rho_s c_s \qquad (5\text{-}2)$$

The effective longitudinal and transverse thermal conductivities, λ_x and λ_y are defined by two components: the bulk thermal conductivity of the porous medium (λ_m) in the absence of groundwater flow and dispersion quantified by the thermal dispersion coefficient (λ_d):

$$\lambda_x = \lambda_m + \lambda_{d,x} \qquad (5\text{-}3)$$

$$\lambda_y = \lambda_m + \lambda_{d,y} \quad (5\text{-}4)$$

1.1.Thermal dispersion

Thermal diffusion and convection are the two main processes involved in the thermal dispersion coefficients given by equations (5-3) and (5-4). Heat transported by temperature gradients within the fluid/solid phase is represented by λ_m. Upon convection the heat is also transported by the moving water itself and differential convection occurs due to the different flow pathways that are possible in porous media. These variations in magnitude and direction of the velocity field at the pore-scale create the so-called thermal dispersion (λ_d) (Bear 1972; Green et al. 1964). In addition, differential heat transport due to the heterogeneity of the permeability field at macroscopic scales also contributes to thermal dispersion (Bear 1972; de Marsily 1986; Ferguson 2007; Hidalgo et al. 2009; Sauty et al. 1982a). Ferguson (2007) and Hidalgo et al. (2009), for instance, emphasize that thermal dispersion is linked to the spatial variability of the hydraulic conductivity field which causes considerable uncertainty about the spreading of the heat plumes in the subsurface.

Traditionally, thermal dispersion has been neglected in heat transport simulation problems because of the dominance of thermal diffusion ($\lambda_m/\rho_m c_m$) (Bear 1972; Fujii et al. 2005; Woodbury and Smith 1985). This is reflected by remarkable thermal diffusion coefficients, which are commonly much higher than those coefficients describing solute diffusion (Bear 1972; Woodbury and Smith 1985). Typical values of solute diffusion coefficients for small molecules are in the order of 10^{-9} m^2/s, whereas values for thermal diffusion coefficient are in the order of 10^{-7} m^2/s (Domenico and Schwartz 1998). One further argument for such simplification is the higher computational effort for numerical modeling of dispersive heat transport. In addition, acquisition of reliable thermal dispersion values would imply additional field measurements and/or calibration procedures.

Thermal dispersion coefficient is usually assumed to be dependent on the fluid velocity and particle size of the porous media (Green et al. 1964; Hsu and Cheng 1990; Lu 2009; Metzger et al. 2004; Pedras and de Lemos 2008; Levec and Carbonell 1985). Metzger et al. (2004), for instance, estimated thermal dispersion coefficients under different fluid velocities scenarios for a packed bed (40 cm × 10 cm) of glass spheres (d = 2 mm). Based on their experimental results, they proposed the following correlations:

$$\frac{\lambda_x}{\lambda_w} = \frac{\lambda_m}{\lambda_w} + APe^{m_1} \tag{5-5a}$$

$$\frac{\lambda_y}{\lambda_w} = \frac{\lambda_m}{\lambda_w} + APe^{m_1} \tag{5-5b}$$

where A = 0.073 and m_1 = 1.59 for the longitudinal dispersion correlation (λ_x/λ_w) and A = 0.03 (lower limit) or 0.05 (upper limit) and m_1 = 1.00 for the transverse dispersion correlation (λ_y/λ_w). The Peclet number (Pe) which relates the energy transported by advection to the energy transported by conduction is expressed in equation (5-5) as:

$$Pe = \frac{\rho_w c_w q d}{\lambda_w} \tag{5-6}$$

where d denotes the mean particle diameter.

Although these kinds of correlations are well accepted in engineering applications, they are uncommon in geothermal modeling. This is mainly due to the fact that they are based on controlled lab experiments with homogenous porous media and the uncertainty introduced by macroscale heterogeneities of hydraulic conductivity is not accounted for. Sauty et al. (1982b) and de Marsily (1986) proposed a thermal dispersion coefficient, similar to solute transport (Bear 1972), where the thermal dispersion term is related to the heterogeneity of the velocity field and is a linear function of this velocity. The following expressions are used by modelers to represent what they do not know about the exact structure of the aquifer and its heterogeneity (Smith and Chapman 1983; Hopmans et al. 2002; Constantz 2008; Molson et al. 1992; Sauty et al. 1982a):

$$\lambda_x = \lambda_m + \alpha_x \rho_w c_w q \tag{5-7}$$

$$\lambda_y = \lambda_m + \alpha_y \rho_w c_w q \tag{5-8}$$

The degree of the thermal dispersion coefficient depends on the direction relative to flow. In two dimensions, this is reflected by two dispersivity terms, a longitudinal (α_x) and a transverse (α_y). The relationship of $\alpha_y = 0.1\alpha_x$ is commonly assumed for solute transport (Domenico and Schwartz 1998; Gelhar et al. 1992), and also for thermal transport (e.g., Molson et al. 1992; Smith and Chapman 1983;

Su et al. 2004; Hopmans et al. 2002). However, this relationship might vary depending on the heterogeneity structure of the aquifer (Beyer et al. 2006) and the Peclet number (Domenico and Schwartz 1998; Bear 1972; Nield and Bejan 2006).

In the area of solute transport, numerous studies on theoretical and experimental investigations were carried out on dispersion in aquifers (Gelhar et al. 1992; Beyer et al. 2006; Xu and Eckstein 1995; Schulze-Makuch 2005; Neuman 1990). They indicate that the solute longitudinal dispersivities are scale dependent (i.e. dispersion depends on the distance traveled by the solute particle). Hence, in the literature some equations relating the field scale and the solute longitudinal dispersivity can be found. In general, they are expressed by the following empirical relationship (Xu and Eckstein 1995; Schulze-Makuch 2005; Neuman 1990):

$$\alpha_x = b(L)^{m_2} \tag{5-9}$$

where L represents the field scale, and b and m_2 characteristic coefficients of the geological medium. Results from different empirical equations are plotted in Figure 5-1. Obviously a large range and uncertainty depending on the applied relationship exists. For instance, using a field scale of 10 m, the longitudinal dispersivity might be 0.5 m, 0.8 m or 2 m, depending entirely on the applied empirical relationship.

Measured and experimental thermal longitudinal dispersivity values reported in the literature (Andrews and Anderson 1979; Constantz et al. 2003; de Marsily 1986; Gelhar et al. 1992; Hatch et al. 2006; Sauty et al. 1982a; Smith and Chapman 1983; Su et al. 2004) are shown in Figure 5-1. Most of these values are located within the ranges given by the empirical relationships derived for solute transport. This also reflects that geological conditions can be highly variable with different representative values of thermal dispersivity.

Windqvist and Hyden (1976), cited in Sauty et al. (1982a), carried out a comparison between heat and solute transport in a Swedish aquifer. The results indicated similar dispersivities for both processes. Sauty et al. (1982a) developed in-situ experimental investigations of hot water storage in a confined aquifer and determined values of thermal dispersivity indirectly by model calibration. They stated that the calculated value of thermal dispersivity was of the same order of magnitude as that obtained with a tracer test at the same site. de Marsily (1986) presented a single field experiment with both solute and

thermal tracer tests. He showed that the thermal and solute longitudinal dispersivities are similar and therefore can be used as equivalent parameters. Yuan et al. (1991) carried out a theoretical study on thermal dispersion in porous media. They conclude that thermal dispersion varies over a wide range as a result of heterogeneities. Ferguson (2007) and Hidalgo et al. (2009) related thermal dispersion to the heterogeneity of the hydraulic conductivity field suggesting that thermal dispersion is somehow linked to the field scale. Under steady state conditions, transverse dispersivity is, for instance, related to the variance of the hydraulic conductivity $\sigma^2_{\ln K}$ and the correlation length L_x of an anisotropic Gaussian semivariogram (Hidalgo et al. 2009):

$$\alpha_y = 0.02\sigma^2_{\ln K} L_x \tag{5-10}$$

For the conditions simulated by Hidalgo et al. (2009), transverse dispersivities vary from 2 to 6 m for a model domain of 1000 × 500 × 500 m (*x*,*y*,*z* direction).

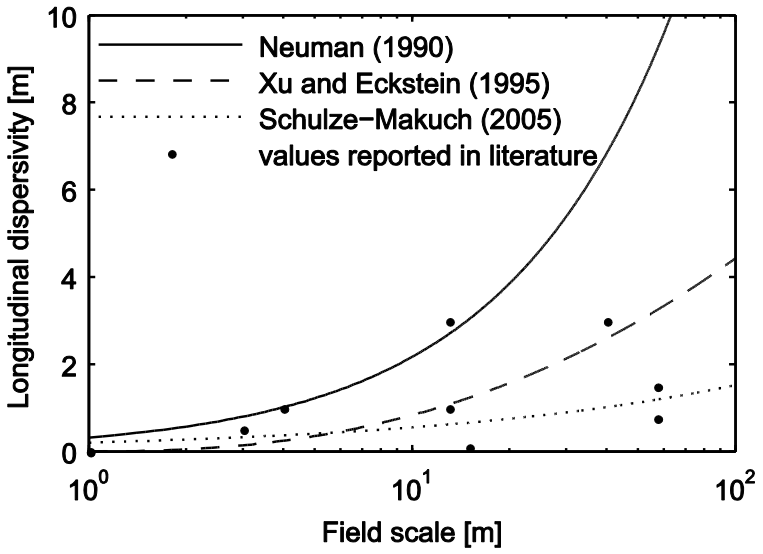

Figure 5-1. Relationship between field scale and solute longitudinal dispersivity for different empirical relationships (solid and intermittent lines). Values of thermal longitudinal dispersivities reported in literature are shown as dots (Andrews and Anderson 1979; Constantz et al. 2003; de Marsily 1986; Gelhar et al. 1992; Hatch et al. 2006; Sauty et al. 1982a; Smith and Chapman 1983; Su et al. 2004)

Vandenbohede et al. (2008) performed two push-pull tests injecting chloride and cold water into an aquifer. Contrary to Windqvist and Hyden (1976) and de Marsily (1986), Vandenbohede et al. (2008) state that thermal and solute dispersivities do not appear to be comparable. Furthermore, they did not

observe a scale dependency for thermal dispersivity. They argue that this is mainly due to the fact that contrary to solute transport, heat is not only transported through the fluid phase, but also throughout the solid phase. Hence, it is less influenced by heterogeneity. Constantz et al. (2003) offer a comparison of heat and solute tracer tests. They claim that thermal dispersivities are notably smaller than solute dispersivities.

In summary, it is still not clear whether the magnitude of the heat and solute dispersivities are the same and whether thermal dispersion is scale-dependent. However, one must have always in mind as explained by Vandenbohede et al. (2008) and Bear (1972) that thermal dispersion in heat transport might be not as significant as in solute transport due to the heat exchange between the fluid and the solid phase. This process is quantified by the retardation factor (R_T) which is given as the ratio between the volumetric heat capacities of the porous medium, $\rho_m c_m$ and water $\theta\rho_w c_w$:

$$R_T = \frac{\rho_m c_m}{\theta \rho_w c_w} \tag{5-11}$$

5.3. Analytical models

The solution of the partial differential equation (PDE) for heat transport in porous media (equation (5-1) for an infinite porous medium with an uniform initial temperature is given by (Metzger et al. 2004):

$$\Delta T(x,y,t) = \frac{q_L}{4\pi\sqrt{\lambda_x \lambda_y}} \exp\left[\frac{\rho_w c_w q x}{2\lambda_x}\right] \int_0^{\frac{(\rho_w c_w q)^2 t}{4\rho c \lambda_x}} \exp\left[-\psi - \left(\frac{x^2}{\lambda_x} + \frac{y^2}{\lambda_y}\right)\frac{(\rho_w c_w q)^2}{16\lambda_x \varphi}\right]\frac{d\psi}{\psi} \tag{5-12}$$

This analytical solution applies for the response of a constant line-source with infinite length along the vertical (*z)* direction with a continuous heat flow rate per unit length of the borehole, q_L. This is a simplified but widely accepted approach to approximate the subsurface heat transport processes stimulated by GSHP operation (Diao et al. 2004; Eskilson 1987; Sutton et al. 2003). Note that although the underground is assumed to be homogeneous in the analytical solution, "artificial" heterogeneity of the hydraulic conductivity field can be accounted for by a thermal dispersion term.

Metzger et al. (2004) used this analytical solution (equation (5-12)) to estimate thermal dispersion coefficients for a packed bed of glass spheres. For steady state conditions, equation (5-12) reduces to the following form:

$$\Delta T(x,y) = \frac{q_L}{2\pi\sqrt{\lambda_x \lambda_y}} \exp\left[\frac{\rho_w c_w q x}{2\lambda_x}\right] K_0\left[\frac{\rho_w c_w q}{2}\sqrt{\frac{\lambda_y x^2 + \lambda_x y^2}{\lambda_x^2 \lambda_y}}\right] \tag{5-13}$$

in which K_0 is the modified Bessel function of the second kind of order zero.

If the thermal dispersion coefficients are set equal to zero ($\lambda_x = \lambda_y = \lambda_m$), equations (5-12) and (5-13) reduce to the following analytical solutions given by Sutton et al. (2003), Zubair and Chaudhry (1996), and Diao et al. (2004):

$$\Delta T(x,y,t) = \frac{q_L}{4\pi\lambda_m} \exp\left[\frac{\rho_w c_w q x}{2\lambda_m}\right] \int_0^{\frac{(\rho_w c_w q)^2 t}{4\rho c \lambda_m}} \exp\left[-\varphi - \frac{(\rho_w c_w q)^2 r^2}{16\lambda_m^2 \varphi}\right] \frac{d\psi}{\psi} \tag{5-14}$$

$$\Delta T(x,y) = \frac{q_L}{2\pi\lambda_m} \exp\left[\frac{\rho_w c_w q x}{2\lambda_m}\right] K_0\left[\frac{\rho_w c_w q r}{2\lambda_m}\right] \tag{5-15}$$

where $r^2 = x^2 + y^2$. Sutton et al. (2003) use this approach to calculate the ground resistance in BHEs. This ground resistance is an indirect measure of how much energy is resisted to flow to the ground. Zubair and Chaudhry (1996) calculate temperature distributions in a homogeneous, isotropic, infinite medium for time-dependent energy extraction/injection. Diao et al. (2004) employ the same equations to evaluate the effect of groundwater advection on GSHP systems.

The calculation of the plume length is complex due to the difficulty of expressing the plume length (L_p) as a function of a specific isotherm contour (ΔT), i.e., $x = f(\Delta T)$. In the present study, an iterative interpolation method is used in MATLAB to compute the temperature plume length for a given ΔT under transient conditions.

For steady state conditions, however, an approximation can be made in order to calculate the length of the temperature plume. Equation (5-13) is first expressed in the following form:

$$\Delta T(L_p,0) = \frac{q_L}{2\pi\sqrt{\lambda_x\lambda_y}} \exp\left[\frac{\rho_w c_w q L_p}{2\lambda_x}\right] K_0\left[\frac{\rho_w c_w q L_p}{2\lambda_x}\right] \tag{5-16}$$

where L_p is the temperature plume length and ΔT is evaluated in the line of symmetry along the x-axis with $y = 0$. The modified Bessel function of the second kind of order zero, $K_0(z)$, can be approximated by the following equation considering only the first two terms of the series expansion (Carslaw and Jaeger 1959):

$$z^{0.5}\exp(z)K_0[z] \approx \sqrt{\frac{\pi}{2}}\left(1-\frac{1}{8z}\right) \tag{5-17}$$

where z is the argument of the Bessel function. Substituting equation (5-17) into equation (5-16) gives the following quadratic equation:

$$\left(\frac{4\pi\rho_w c_w \lambda_y q \Delta T^2}{{q_L}^2}\right){L_p}^2 - L_p + \frac{\lambda_x}{2\rho_w c_w q} = 0 \tag{5-18}$$

Finally, solving equation (5-18) for the temperature plume length (L_p) yields:

$$L_p = \left(\frac{{q_L}^2}{8\pi\rho_w c_w \lambda_y q \Delta T^2}\right)\left(1 \pm \sqrt{1-\frac{8\pi\lambda_x\lambda_y\Delta T^2}{{q_L}^2}}\right) \tag{5-19}$$

Equation (5-19) can be used to calculate the length of a temperature plume (L_p) for a given isothermal contour (ΔT) under steady state conditions. This approximation, however, is valid only for z >> 1. The relative error of the approximation is within 0.01 when z > 3 (Abramowitz and Stegun 1964). As an example, Figure 5-2 shows a comparison of the approximation equation (equation (5-19)) with the full solution (equation (5-16)). For this specific case, the relative error is about 5% for a ΔT = -2 K and for ΔT > -1.4 K the relative error is lower than 1%.

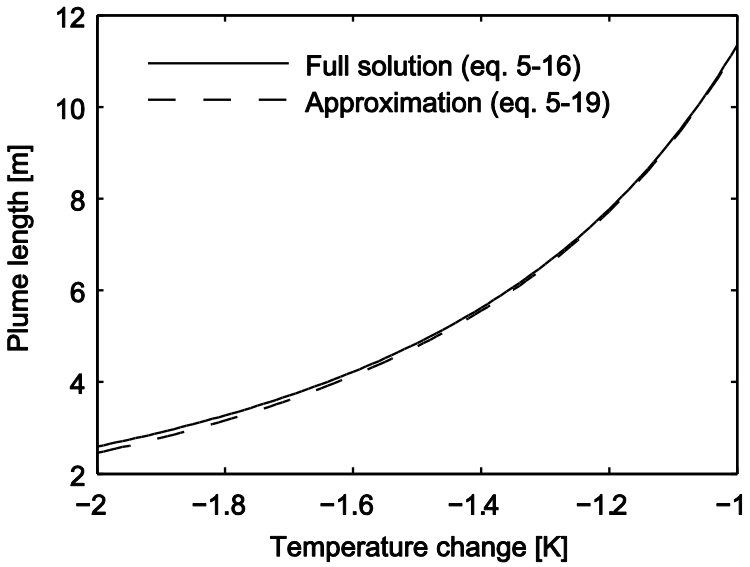

Figure 5-2. Plume length for steady state conditions as a function of temperature change: Small discrepancies are observed between the predictions by the temperature plume length equation and by the full solution ($q = 2 \times 10^{-6}$ m/s, $\lambda_x = 7$ W/m/K, , $\lambda_y = 3$ W/m/K, $q_L = -60$ W/m, $y = 0$ m).

5.4. Model set up

For the evaluation of the effect of thermal dispersion on temperature plumes, a 2D synthetic model is set up and solved analytically for transient and steady state conditions using equations (5-12)- (5-13). Table 5-1 provides typical hydraulic and thermal parameters for natural aquifer systems (VDI 2000; de Marsily 1986; Spitz and J. Moreno 1996). Hydraulic conductivities show a wide range over more than 8 orders of magnitude. In contrast, the variability of heat transport parameters is comparatively low.

Table 5-1. Hydraulic and thermal parameters for unconsolidated aquifer materials. Hydraulic conductivity, Darcy velocity, bulk thermal conductivity and volumetric heat capacity of porous medium are represented by K, q, λ_m and $\rho_m c_m$, respectively. q is calculated based on an hydraulic gradient of 10^{-3}. Values for λ_m and $\rho_m c_m$ are for saturated aquifer materials.

Aquifer material	K [m/s]	q [m/s]	λ_m [W/m/K]	$\rho c \times 10^6$ [J/m^3/K]
Gravel	$10^{-4} – 10^{-2}$	$10^{-7} – 10^{-5}$	1.8	2.4
Coarse sand	10^{-3}	10^{-6}	1.7 – 5.0	2.2 – 2.9
Medium sand	10^{-4}	10^{-7}	1.7 – 5.0	2.2 – 2.9
Fine sand	$10^{-6} –10^{-5}$	$10^{-9} – 10^{-8}$	1.7 – 5.0	2.2 – 2.9
Silt	10^{-7}	10^{-10}	0.9 – 2.3	1.6 – 3.4
Clay	$10^{-10} – 10^{-9}$	$10^{-13} – 10^{-12}$	1.2 – 1.5	2.3

Due to their low variability in nature, values of some thermal model parameters are fixed. Thermal conductivity and heat capacity of the bulk porous media are set to 2.5 W/m/K and 2.8×10^6 J/m^3/K,

respectively. Accordingly, the thermal diffusivity is set to 9×10^{-7} m/s. These values are within the range of typical sand aquifers (de Marsily 1986; VDI 2000).

The influence of the other descriptive parameters is further scrutinized. Several groundwater flow scenarios are evaluated by varying hydraulic conductivity from 10^{-5} m/s to 10^{-2} m/s, which is within the range for typical sand and gravel aquifers (Table 5-1). Assuming a constant hydraulic gradient of 10^{-3}, the Darcy velocity (q) ranges from 10^{-8} m/s to 10^{-5} m/s. Darcy velocities lower than 10^{-8} m/s are not considered here, because thermal dispersion is expected to have only a minor effect under such conditions. Energy extraction is set to a typical value of -60 W/m, based on 2400 h (100 days) of operation during the year in a sand and gravel aquifer (VDI 2001).

As reviewed above, there is some controversy regarding the scale dependence of thermal dispersivity and its similarity with solute dispersivity. Therefore, two assumptions are made: 1) thermal dispersion is assumed to be only dependent on the Darcy velocity (e.g., homogeneous aquifers). Hence, relationships proposed by Metzger et al. (2004) are used and 2) thermal dispersion is assumed to be comparable to solute dispersion and scale-dependent.

In order to relate the thermal dispersion correlations given by equation (5-5) with the dispersivity terms (α_x, α_y), Equation (5-5) is compared with equations (5-7) and (5-8). This yields the following expression:

$$\alpha_{x,y} = A\left(\frac{\rho_w c_w q}{\lambda_w}\right)^{m_1-1} d^{m_1} \tag{5-20}$$

For the present study an upper limit of the Darcy velocity of 1×10^{-5} m/s is set, which represents a rather high velocity in natural porous aquifers. Assuming a particle diameter of 0.065 m, which is the maximum value for gravel, results in a longitudinal and transverse dispersivity of $\alpha_x = 1 \times 10^{-2}$ m (1 cm) and $\alpha_y = 3.3 \times 10^{-3}$ m (0.33 cm), respectively. These values are used for the first approach.

For the second approach, a field scale of 10 m distance downgradient from the point of energy extraction is chosen. This distance is based on the recommended minimum distance between two BHEs in the state of Baden-Württemberg, Germany (Hähnlein et al. 2010b). For a field scale of 10 m, longitudinal dispersivities vary from 0.5 m to 2 m depending on the applied empirical relationship

(Figure 5-1). For the sake of simplicity, transverse dispersivities are set between 0.05 m and 0.2 m, assuming $\alpha_y = 0.1\alpha_x$ (Hopmans et al. 2002; Molson et al. 1992; Smith and Chapman 1983; Su et al. 2004). A summary of the resulting scenarios is presented in Table 5-2.

Table 5-2. Dispersivity range scenarios. Scenario 1: thermal dispersion is assumed to be only dependent on the Darcy velocity (REV: Representative elementary volume). Scenario 2: thermal dispersion is assumed to be scale dependent.

scenario	dispersivity	field scale
1	$\alpha_x = 1 \times 10^{-2}$ m $\alpha_y = 3.3 \times 10^{-3}$ m	REV
2	$\alpha_x = 0.5 – 2.0$ m $\alpha_y = 0.05 – 0.2$ m	10 m

In order to assess the influence of thermal dispersion on the simulation of temperature plumes, simulations of temperature profiles along the centerline of the plume are carried out for a distance of 1 m – 10 m downgradient from the source for steady state and transient conditions. The simulations are run for the range of Darcy velocities and thermal dispersivities as given above. An example of a temperature profile for steady state conditions is shown in Figure 5-3.

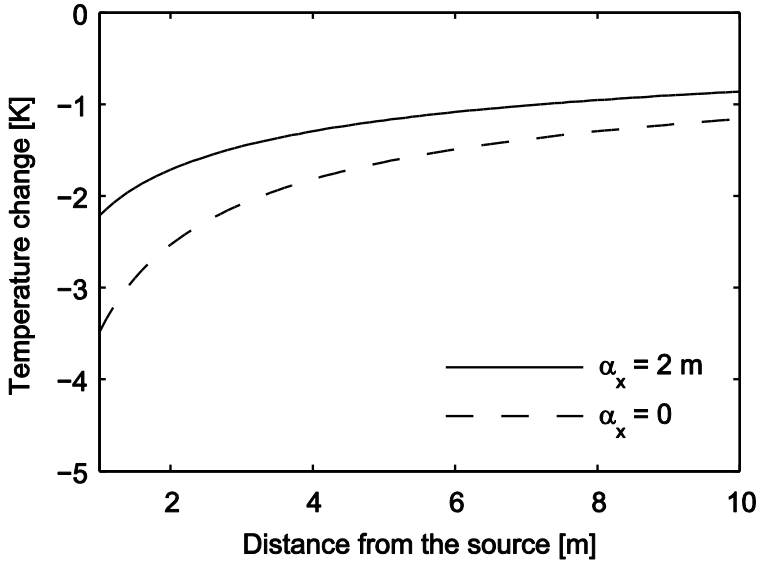

Figure 5-3. Temperature profiles along the centerline for steady state conditions with and without thermal dispersion ($q = 2 \times 10^{-6}$ m/s, $y = 0$ m). RMSE = 0.56 K (equation (5-21)).

Comparison of the results is based on the computed root mean square error (RMSE) which quantifies the residual error of the temperature profiles between the outputs with and without thermal dispersion as follows:

$$\mathrm{RMSE} = \sqrt{\frac{\sum_{i=1}^{n}\left(\Delta T_{o(i)} - \Delta T_{(i)}\right)^2}{n}} \tag{5-21}$$

in which $\Delta T_{(i)}$ corresponds to the results from the analytical solution considering thermal dispersion (which are considered as 'true' values), and $\Delta T_{o(i)}$ corresponds to the results from the analytical solution with only diffusion ($\lambda_d = 0$). As an empirical threshold, we consider that RMSE values < 0.1 K represent conditions in which the influence of thermal dispersion is marginal enough to be ignored. This is based on the typical measurement accuracy of temperature.

5.5. Results and discussion

5.5.1. Effect of thermal dispersion on the temperature response

Discrepancies of the temperature response distribution for steady state conditions are depicted by contour maps of root mean square error (RMSE) for a bulk thermal conductivity of the porous medium of 2.5 W/m/K (Figure 5-4a) and 4.0 W/m/K (Figure 5-4b). The contours delineate the RMSE of the temperature change with and without thermal dispersivity for a distance of 1 m to 10 m downgradient from the source in dependence on Darcy flow velocity. As expected, the larger the neglected thermal dispersivity, the larger the RMSE of the calculated temperature distribution. What is more, the error also increases with rising Darcy velocities (Figure 5-4). This reflects the effect of the thermal dispersion on the temperature plume distribution in steady state conditions. It has to be mentioned, however, that for high dispersivity and Darcy velocity scenarios (α_x > 1 m; $q > 5 \times 10^{-6}$ m/s), the RMSE slightly decreases. Under these conditions, the temperature profile becomes quite flat due to the dissipated energy and therefore the RMSE decreases.

Ignoring longitudinal dispersivities of less than 0.1 m yields RMSE values lower than 0.1 K. Therefore, for the range of flow velocities taken in this study, the influence of thermal dispersion given by scenario 1 ($\alpha_x = 1 \times 10^{-2}$ m) is marginal enough to be ignored. In this sense, if we assume that macroscopic heterogeneities of the hydraulic conductivity field do not have an effect on the thermal

dispersion (i.e., homogeneous aquifer), then thermal dispersion given only by the dependence on the Darcy velocity has no major influence on the temperature plume distribution.

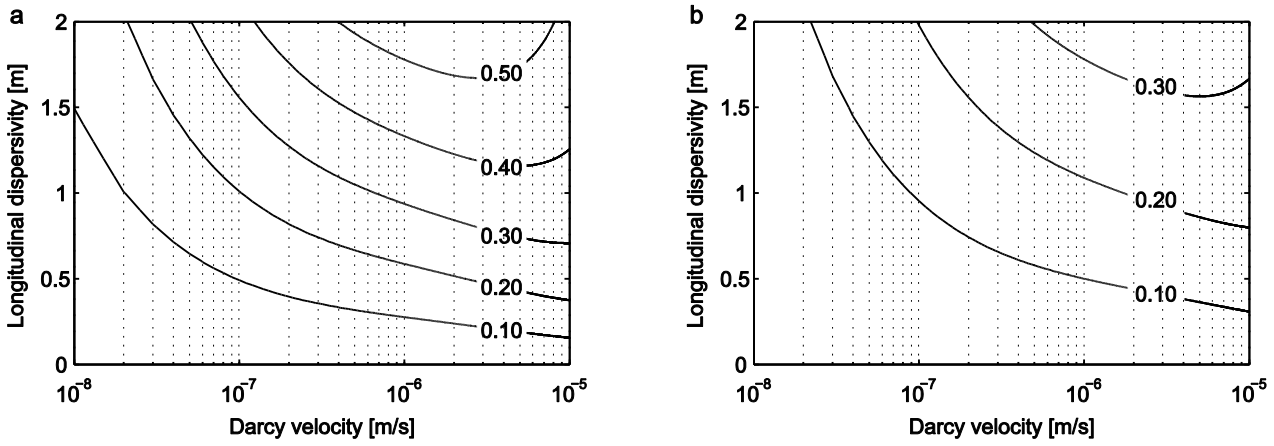

Figure 5-4. Contour maps of RMSE [K] in dependence on Darcy velocity for steady state conditions with and without thermal dispersion (downgradient distance range x = 1 m – 10 m): (a) λ_m = 2.5 W/m/K, (b) λ_m = 4.0 W/m/K

For the range of thermal dispersivities given by scenario 2 (α_x = 0.5 – 2 m), the RMSE varies up to 0.56 K for λ_m = 2.5 W/m/K depending on the Darcy velocity. For this specific case, only for Darcy velocities around 10^{-8} m/s the RMSE is less than 0.1 K for most of the dispersivity range. For larger velocities, the error can be higher than 0.1 K. For instance, if thermal dispersion if neglected for a longitudinal dispersivity of 2 m and a Darcy velocity of 1×10^{-6} m/s, the RMSE is about 0.56 K, which is about 23% of the maximum temperature change (2.4 K) in the temperature profile (Figure 5-3). In order to evaluate the effect of the thermal conductivity when neglecting thermal dispersion, a higher value of λ_m (4.0 W/m/K) is assumed (Figure 5-4b). As we can see, an increase in thermal conductivity results in a lower effect of neglecting thermal dispersion. For instance, neglecting a thermal dispersivity of 1.5 m with a $q = 1 \times 10^{-8}$ m/s yields an RMSE = 0.1 K for a thermal conductivity of 2.5 W/m in steady state conditions, whereas for a higher thermal conductivity of 4.0 W/m, the same Darcy velocity yields an RMSE << 0.1 K.

For transient conditions, the discrepancies of the temperature plume distribution are shown in Figure 5-5 for different aquifer materials. Fine sand, medium sand, coarse sand and gravel aquifers are evaluated with a Darcy velocity of 10^{-8} m/s, 10^{-7} m/s, 10^{-6} m/s and 10^{-5} m/s, respectively. Moreover, the selected simulation times are based on the instant when longitudinal dispersion is more dominant over

the transverse one at a distance of 10 m for each Darcy velocity (Figure 5-6). Similar to steady state conditions, under transient conditions the influence of thermal dispersion based on scenario 1 is minor. For scenario 2, it can be seen that the RMSE varies up to 0.6 K. Only for Darcy velocities of 10^{-8} m/s is the RMSE less than 0.1 K for the whole range of neglected longitudinal dispersivity. For Darcy velocities of 10^{-7} m/s, the RMSE only exceeds 0.1 K for longitudinal dispersivities larger than 0.8 m. On the other hand, for coarse sand and gravel aquifers (10^{-6} m/s, 10^{-5} m/s) the RMSE increases up to 0.6 K. These results, however, might vary depending on the examined transient times.

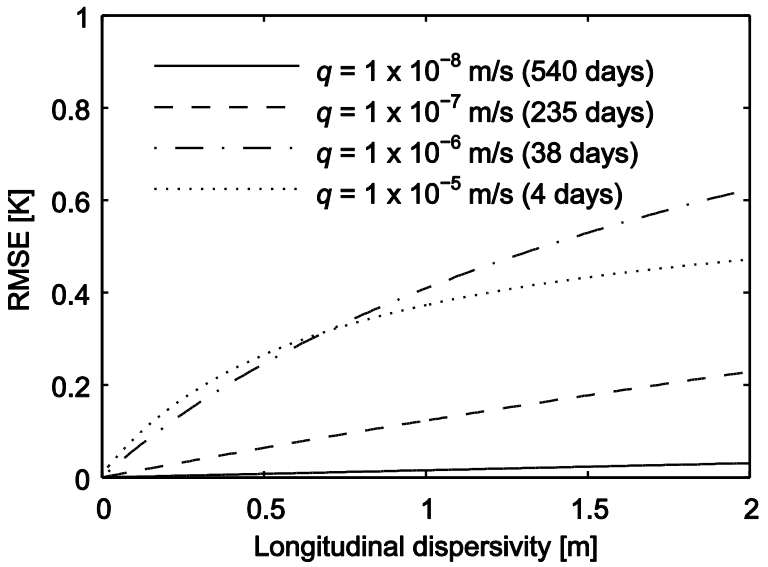

Figure 5-5. RMSE as a function of Darcy velocity for transient conditions with and without thermal dispersion. Fine sand, medium sand, coarse sand and gravel aquifers are simulated with a Darcy velocity of 10^{-8} m/s, 10^{-7} m/s, 10^{-6} m/s and 10^{-5} m/s, respectively (x = 1 m – 10 m, λ_m = 2.5 W/m/K).

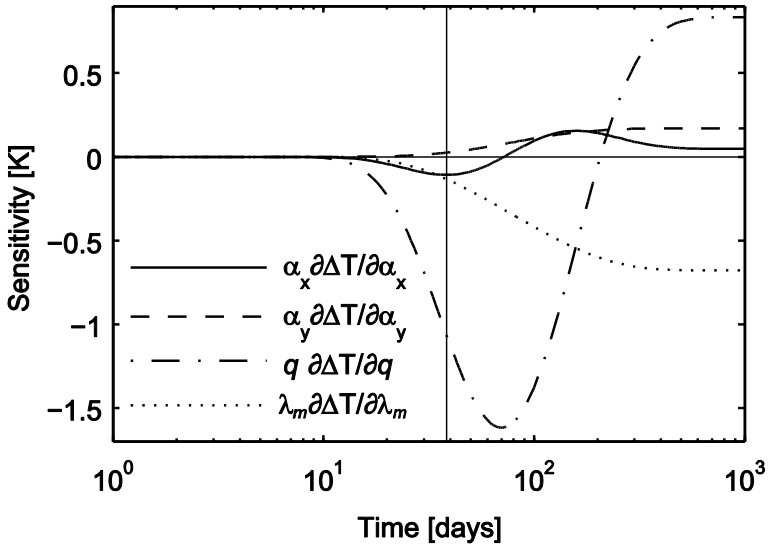

Figure 5-6. Relative sensitivities of equation (5-12) at a distance of 10 m downgradient from the source ($q = 1 \times 10^{-6}$ m/s). It shows the sensitivity of the temperature change (ΔT) to variations of the longitudinal dispersivity α_x, transverse dispersivity α_y, bulk thermal conductivity of porous medium λ_m, and Darcy velocity q as a function of time.

5.5.2. Development of the temperature plume length

The analytical equation for steady-state conditions (equation (5-13)) is computed in two dimensions. Figure 5-7 depicts relative temperature contours (isotherms) for different values of thermal dispersivity. Relative temperature means that the isotherms delineate a temperature difference of ΔT = -1 K between plume and ambient conditions. It can be observed that the temperature plume gets shorter with increasing dispersivity. This is attributed to the fact that for steady state conditions, longitudinal dispersivity is not as important as the transverse one. For long time simulation, the relative sensitivity of longitudinal dispersivity almost disappears while transverse dispersivity reaches its maximum in equation (5-12) (Figure 5-6). Hence, spreading of heat in the transverse direction to flow causes dissipation of energy. Apparently, a dispersion-dominated regime yields lower temperature changes close to the source, i.e. the BHE, in steady state conditions in comparison to scenarios without thermal dispersion. Therefore, neglecting thermal dispersion results in an overestimation of the temperature plume length under steady state conditions.

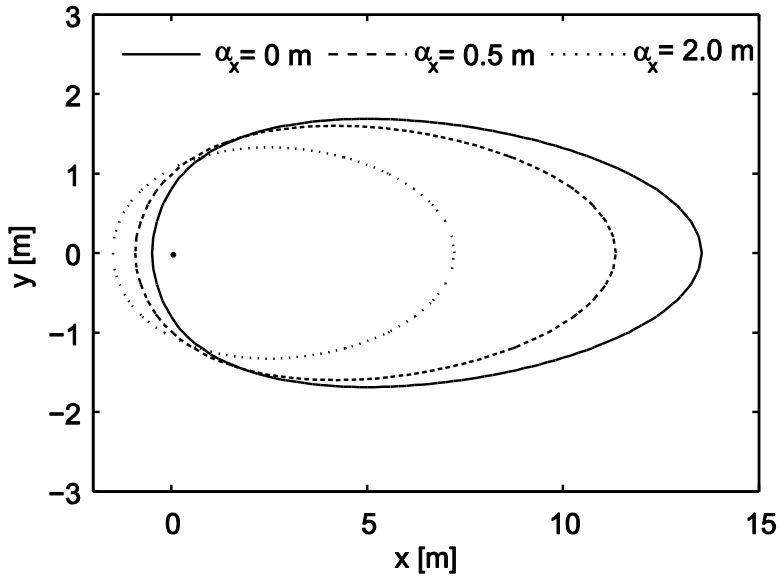

Figure 5-7. Temperature plumes in steady state conditions for different thermal dispersivities in a coarse sand aquifer (ΔT = -1 K, $q = 2.0 \times 10^{-6}$ m/s).

For transient conditions some temperature isotherms can reach greater distances when increasing thermal dispersion. Figure 5-8, for instance, shows that neglecting a thermal dispersivity of 2 m with a Darcy velocity of 3×10^{-7} m/s results in an underestimation of the temperature plume length of around 1 m. This is due to the dominance of longitudinal dispersion over the transverse dispersion at this specific point for transient conditions.

Figure 5-8 shows the behavior of the temperature plume length as a function of Darcy velocity. For the specific case shown in this figure (t = 50 days, ΔT = -0.5 K), we can see that the temperature plume length first increases over a range of velocities in which there are still transient conditions and the longitudinal dispersion prevails over the transverse one. Then, there is a transition between transient and steady state conditions and finally the temperature plume decreases as higher values of Darcy velocity are assumed.

For a Darcy velocity of 7.0×10^{-6} m/s, the heat plume for a temperature change of -0.5 K is 4 m long considering a longitudinal dispersivity of 2 m. Ignoring the thermal dispersivity, the calculated plume length is 15 m. Such a discrepancy can be critical for licensing GSHP systems, e.g. if the suggested distance between neighboring boreholes is 10 m.

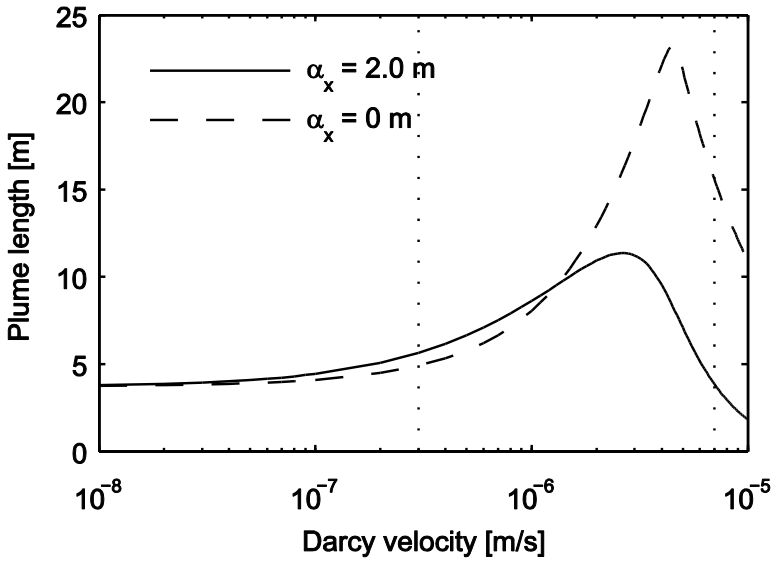

Figure 5-8. Plume length as a function of the Darcy velocity (λ_m = 2.5 W/m/K, q_L = -60 W/m, t = 50 days, ΔT = -0.5 K).

5.6. Conclusions

An analytical modeling study of the effect of neglecting thermal dispersion under different groundwater flow and dispersion conditions is carried out. For this purpose, analytical solutions to simulate heat transport in the subsurface for steady state and transient conditions are applied. Moreover, an equation to calculate the length of the temperature plume for steady state is developed. Our criterion for assessing the influence of thermal dispersion on the temperature plumes created by the use of GSHP systems is the calculated error that would be introduced. Therefore, the root mean square error (RMSE) is taken to quantify the discrepancy between results with and without thermal dispersion. The RMSE rises with increasing values of the ignored thermal dispersivity. What is more, it also increases with larger Darcy velocities.

It has to be mentioned that a fixed hydraulic gradient of 10^{-3} was assumed. Therefore, the results are based on this assumption. For homogenous aquifers in which the thermal dispersion depends only on the magnitude of groundwater flow, the effect of thermal dispersion on the temperature plume distribution around the BHE is minor (RMSE << 0.1 K) under steady state and transient conditions. On the other hand, if thermal dispersion is assumed to be scale-dependent and if the development of the temperature profiles and the extension of the temperature plumes are of concern, neglecting thermal dispersion is critical for conditions typical for medium sand to gravel aquifers (with Darcy velocities q

> 10^{-8} m/s) for steady state and transient conditions. For geological conditions dominated by fine sand ($q = 10^{-8}$ m/s), the assumption of neglecting thermal dispersion must be carefully evaluated depending on the case-specific thermal conductivity and thermal dispersivity. An increase in thermal conductivity results in a lesser effect of ignoring thermal dispersion.

Thermal dispersion causes dissipation of energy. Temperature plume lengths become shorter with increasing thermal dispersion for steady state conditions. Apparently, a dispersion-dominated regime yields lower temperature changes close to the source, i.e. the BHE, in comparison to scenarios without thermal dispersion. For transient conditions, however, temperature plume lengths for certain isotherms can become larger with increasing thermal dispersion.

We can conclude that the consideration of the thermal dispersion is an important factor regarding the temperature plumes in the subsurface that develop from GSHP systems for sand and gravel aquifers. From the perspective of environmental regulators, such assumptions might be crucial for licensing applications and sustainable operation of neighboring GSHP systems. In comparison, ignoring thermal dispersion provides appropriate predictions of the extension and shape of temperature plumes for flow conditions typical for geological formations dominated by fine sands, clays, and silts with $q < 10^{-8}$ m/s. Accordingly, the range of hydrogeological conditions in which the thermal dispersivity can be ignored is still large. This might be the reason why thermal dispersion has been traditionally neglected in heat transport simulation problems.

It has to be mentioned here that the presented results are based on the selected RMSE (root mean square error) threshold (RMSE > 0.1 K). In addition, it should be kept in mind that errors related to the determination of hydraulic conductivity (Lessoff et al. 2010) might lead to higher uncertainty in the determination of temperature plumes than those related to neglecting thermal dispersion.

Finally, the range of dispersivity values chosen in this study is based on a field scale of 10 m. For larger distances and assuming scale-dependency, thermal dispersivities can be higher and consequently have greater influence on the extension of the simulated temperatures plumes and induced temperature changes.

6. Summary and concluding remarks

Conceptual simplifications of processes and boundary conditions describing heat transport in the subsurface are often assumed but rarely discussed. In the present PhD thesis, a comprehensive study of simplifications such as thermal dispersion in aquifers and axial effects was carried out. Attention has been focused on the heat transport simulation in the underground in the area of heat as a tracer and shallow geothermal energy.

Chapter 1 and 2 consists of a general overview of the use of natural temperature fluctuations as a heat tracer and low-enthalpy geothermal energy and Chapters 3-5 present the principal results of the PhD thesis. Chapter 3 used numerical and analytical methods to evaluate the propagation of seasonal temperature signals into an aquifer upon bank infiltration. Simplifications of physical processes in the conceptual model are evaluated in order to assess the importance of different system elements. In general, the temperature signal distribution in shallow aquifer is significant influenced by diffusion of heat into the unsaturated zone and the underlying aquitard. Hence, simplified numerical conceptualizations or analytical models might produce misleading results depending on the groundwater velocity and the thickness of the confining layers. For practical applications of heat as a tracer is therefore recommendable to perform preliminary simulations that includes diffusion transfer process into confining layers to assess whether simplified models are valid for a given travel distance.

Conduction into confining layers is further scrutinized in Chapter 4 for a specific application in geothermal energy. Influence of axial effects is estimated by evaluating the heat transfer at the borehole heat exchanger for ground source heat pump systems. In order to do so, a new analytical approach which accounts for groundwater flow, constant surface temperature and vertical heat losses is proposed. Results showed that the role of axial effects mainly depends on the magnitude of the groundwater velocity in the aquifer and the length of the borehole heat exchanger. In general, for Peclet numbers between 1.2 and 10 the combined effect of groundwater flow and vertical heat losses must be accounted for. For larger Peclet numbers, axial effects can be neglected due to the predominance of advective heat transport in the horizontal direction.

Finally, in Chapter 5 the effect of neglecting thermal dispersion is addressed. In this particular case, similar to Chapter 4, ground source heat pump systems are used as a practical example. For this purpose, existing analytical solutions to simulate heat transport in the subsurface are applied. Influence of thermal dispersion on the temperature plume distribution that evolves from GSHP systems is evaluated for different scenarios by varying the groundwater velocity and the dispersivity coefficient. The results showed that the consideration of thermal dispersion is an important factor regarding the temperature plumes in the subsurface for sand and gravel aquifer when thermal dispersivity is assumed to be scale-dependent. From the perspective of environmental regulators such assumptions might be important for licensing applications of neighboring GSHP systems.

References

Abramowitz, M., and I.S. Stegun. 1964. *Handbook of mathematical functions. With formulas, graphs and mathematical tables*. New York: Dover Publications Inc.

Anderson, M.P. 2005. Heat as a ground water tracer. *Ground Water* 43 no. 6: 951–968.

Andrews, C.B., and M.P. Anderson. 1979. Thermal alteration of groundwater caused by seepage from a cooling lake. *Water Resour. Res.* 15 no. 3: 595-602.

Bandos, T.V., Á. Montero, E. Fernández, J.L.G. Santander, J.M. Isidro, J. Pérez, P.J.F. de Córdoba, and J.F. Urchueguía. 2009. Finite line-source model for borehole heat exchangers: effect of vertical temperature variations. *Geothermics* 38 no. 2: 263–270.

Barlow, J.R.B., and R.H. Coupe. 2009. Use of heat to estimate streambed fluxes during extreme hydrologic events. *Water Resour. Res.* 45 no. 1: W01403, doi:10.1029/2007WR006121.

Bear, J. 1972. *Dynamics of Fluids in Porous Media*. New York: American Elsevier Publishing Company Inc.

Bense, V.F., and H. Kooi. 2004. Temporal and spatial variations of shallow subsurface temperature as a record of lateral variations in groundwater flow. *J. Geophys. Res.* 109 no. B4: B04103, doi:10.1029/2003JB002782, 2004.

Beyer, C., S. Bauer, and O. Kolditz. 2006. Uncertainty assessment of contaminant plume length estimates in heterogeneous aquifers. *J. Contam. Hydrol.* 87 no. 1-2: 73–95.

Blasch, K.W., T.P.A. Ferré, J.P. Hoffmann, and J.B. Fleming. 2006. Relative contributions of transient and steady state infiltration during ephemeral streamflow. *Water Resour. Res.* 42 no. 8: W08405, doi:10.1029/2005WR004049.

Blum, P., G. Campillo, W. Münch, and T. Kölbel. 2010. CO_2 savings of ground source heat pump systems - A regional analysis. *Renew. Energ.* 35 no. 1: 122–127.

Bracewell, R.N. 2000. *The Fourier Transform and its applications*. 3d ed. New York: McGraw-Hill International Editions.

Bravo, H.R., F. Jiang, and R.J. Hunt. 2002. Using groundwater temperature data to constrain parameter estimation in a groundwater flow model of a wetland system. *Water Resour. Res.* 38 no. 8: 1153, doi:10.1029/2000WR000172.

Bredehoeft, J.D., and I.S. Papaopulos. 1965. Rates of vertical groundwater movement estimated from the Earth's thermal profile. *Water Resour. Res.* 1 no. 2: 325–328.

Brooks, A.N., and T.J.R. Hughes. 1982. Streamline upwind/Petrov-Galerkin formulations for convection dominated flows with particular emphasis on the incompressible Navier-Stokes equations. *Comput. Method. Appl. M.* 32 no. 1-3: 199–259.

Bundschuh, J. 1993. Modeling annual variations of spring and groundwater temperatures associated with shallow aquifer systems. *J. Hydrol.* 142 no. 1-4: 427–444.

Carsel, R., and R. Parrish. 1988. Developing Joint Probability Distributions of Soil Water Retention Characteristics. *Water Resour. Res.* 24 no. 5: 755–769.

Carslaw, H.S., and J.C. Jaeger. 1959. *Conduction of Heat in Solids*. 2nd ed. New York: Oxford University Press.

Chaudhry, M.A., and S.M. Zubair. 1994. Generalized incomplete gamma functions with applications. *J. Computational Appl. Math.* 55 no. 1: 99–123.

Chiasson, A.D., S.J. Rees, and J.D. Spitler. 2000. A preliminary assessment of the effects of ground water flow on closed-loop ground-source heat pump systems. *ASHRAE Trans.* 106 no. 1: 380–393.

Cirpka, O.A., N.F. Michael, H. Markus, H. Eduard, T. Aronne, K. Rolf, and K.K. Peter. 2007. Analyzing Bank Filtration by Deconvoluting Time Series of Electric Conductivity. *Ground Water* 45 no. 3: 318–328.

Clauser, C. 2006. *Geothermal Energy, In: K. Heinloth (Ed), Landolt-Börnstein – Numerical Data and Functional Relationships, New Series, Vol. VIII: Energy Technologies, Subvolume 3: Renewable Energies, Springer Verlag, Heidelberg-Berlin.*

Conant, B.J. 2004. Delineating and quantifying ground water discharge zones using streambed temperatures. *Ground Water* 42 no. 2: 243–257.

Constantz, J. 1998. Interaction between stream temperature, streamflow, and groundwater exchanges in Alpine streams. *Water Resour. Res.* 34 no. 7: 1609–1616.

———. 2008. Heat as a tracer to determine streambed water exchanges. *Water Resour. Res.* 44, no. 12: W00D10, doi:10.1029/2008WR006996, 2008.

Constantz, J., M.H. Cox, and G.W. Su. 2003. Comparison of Heat and Bromide as Ground Water Tracers Near Streams. *Ground Water* 41 no. 5: 647–656.

Constantz, J., A.E. Stewart, R. Niswonger, and L. Sarma. 2002. Analysis of temperature profiles for investigating stream losses beneath ephemeral channels. *Water Resour. Res.* 38 no. 12: 1316, doi:10.1029/2001WR001221.

De Carli, M., M. Tonon, A. Zarrella, and R. Zecchin. 2010. A computational capacity resistance model (CaRM) for vertical ground-coupled heat exchangers. *Renew. Energ.* 35 no. 7: 1537–1550.

de Marsily, G. 1986. *Quantitative Hydrogeology*. San Diego, California: Academic Press.

DHI-WASY. 2010. *FEFLOW 6- User's Manual. Berlin: DHI-WASY GmbH*.

Diao, N., Q. Li, and Z. Fang. 2004. Heat transfer in ground heat exchangers with groundwater advection. *Int. J. Therm. Sci.* 43 no. 12: 1203–1211.

Domenico, P.A., and F.W. Schwartz. 1998. *Physical and Chemical Hydrogeology*. 2nd ed. New York: John Wiley & Sons Inc.

Duque, C., M.L. Calvache, and P. Engesgaard. 2010. Investigating river-aquifer relations using water temperature in an anthropized environment (Motril-Salobreña aquifer). *J. Hydrol.* 381 no. 1-2: 121–133.

Eskilson, P. 1987. *Thermal analysis of heat extraction boreholes. Ph.D. Thesis. University of Lund, Lund, Sweden*.

Fan, R., Y. Jiang, Y. Yao, and Z. Ma. 2008. Theoretical study on the performance of an integrated ground-source heat pump system in a whole year. *Energy* 33 no. 11: 1671–1679.

Fan, R., Y. Jiang, Y. Yao, D. Shiming, and Z. Ma. 2007. A study on the performance of a geothermal heat exchanger under coupled heat conduction and groundwater advection. *Energy* 32 no. 11: 2199–2209.

Ferguson, G. 2007. Heterogeneity and Thermal Modeling of Ground Water. *Ground Water* 45 no. 4: 485–490.

———. 2009. Unfinished Business in Geothermal Energy. *Ground Water* 47 no. 2: 167–167.

Fujii, H., R. Itoi, J. Fujii, and Y. Uchida. 2005. Optimizing the design of large-scale ground-coupled heat pump systems using groundwater and heat transport modeling. *Geothermics* 34 no. 3: 347–364.

Gelhar, L.W., C. Welty, and K.R. Rehfeldt. 1992. A Critical Review of Data on Field-Scale Dispersion in Aquifers. *Water Resour. Res.* 28 no. 7: 1955–1974.

Goto, S., M. Yamano, and M. Kinoshita. 2005. Thermal response of sediment with vertical fluid flow to periodic temperature variation at the surface. *J. Geophys. Res.* 110 no. 1: B01106, doi:10.1029/2004JB003419.

Green, D.W., R.H. Perry, and R.E. Babcock. 1964. Longitudinal Dispersion of Thermal Energy Through Porous Media with a Flowing Fluid. *AIChE J.* 10 no. 5: 645–651.

Hähnlein, S., N. Molina-Giraldo, P. Blum, P. Bayer, and P. Grathwohl. 2010a. Ausbreitung von Kältefahnen im Grundwasser bei Erdwärmesonden [Cold plumes in groundwater for ground source heat pump systems]. *Grundwasser* 15: 123–33.

Hähnlein, S., P. Bayer, and P. Blum. 2010b. International legal status of the use of shallow geothermal energy. *Renew. Sust. Energ. Rev.* 14: 2611–2625.

Hatch, C.E., A.T. Fisher, J.S. Revenaugh, J. Constantz, and C. Ruehl. 2006. Quantifying surface water-groundwater interactions using time series analysis of streambed thermal records: Method development. *Water Resour. Res.* 42 no. 10: W10410, doi:10.1029/2005WR004787.

Healy, R.W., and A.D. Ronan. 1996. Documentation of Computer Program VS2DH for Simulation of Energy Transport in Variably Saturated Porous Media-Modification of the US Geological Survey´ s Computer Program VS2DT, Water-Resources Investigations Report 96-4230, Denver, Colorado.

Hecht-Méndez, J., N. Molina-Giraldo, P. Blum, and P. Bayer. 2010. Evaluating MT3DMS for heat transport simulation of closed shallow geothermal systems. *Ground Water* 48 no. 5: 741–756.

Hellström, G. 1991. Ground Heat Storage Thermal Analyses of Duct Storage Systems, I. Theory. Ph.D. Thesis, Department of Mathematical Physics, University of Lund, Sweden.

Hidalgo, J.J., J. Carrera, and M. Dentz. 2009. Steady state heat transport in 3D heterogeneous porous media. *Adv. Water Resour.* 32 no. 8: 1206–1212.

Hoehn, E., and O.A. Cirpka. 2006. Assessing residence times of hyporheic ground water in two alluvial flood plains of the Southern Alps using water temperature and tracers. *Hydrol. Earth Syst. Sc.* 10 no. 4: 553–563.

Hopmans, J.W., J. imunek, and K.L. Bristow. 2002. Indirect estimation of soil thermal properties and water flux using heat pulse probe measurements: Geometry and dispersion effects. *Water Resour. Res.* 38 no. 1: 1006, oi:10.1029/2000WR000071.

Hsu, C.T., and P. Cheng. 1990. Thermal dispersion in a porous medium. *Int. J. Heat Mass Tran.* 33 no. 8: 1587–1597.

Ingersoll, L.R., O.J. Zobel, and A.C. Ingersoll. 1954. *Heat conduction with engineering, geological and other applications*. New York: McGraw-Hill.

Keery, J., A. Binley, N. Crook, and J.W.N. Smith. 2007. Temporal and spatial variability of groundwater-surface water fluxes: Development and application of an analytical method using temperature time series. *J. Hydrol.* 336 no. 1-2: 1–16.

Kim, E.-J., J.-J. Roux, G. Rusaouen, and F. Kuznik. 2010. Numerical modelling of geothermal vertical heat exchangers for the short time analysis using the state model size reduction technique. *Appl. Therm. Eng.* 30 no. 6-7: 706–714.

Kupfersberger, H. 2009. Heat transfer modelling of the Leibnitzer Feld aquifer, Austria. *Environ. Earth Sci.* 59 no. 3: 561–571.

Lamarche, L., and B. Beauchamp. 2007. A new contribution to the finite line-source model for geothermal boreholes. *Energ. Buildings* 39 no. 2: 188–198.

Langguth, H.-R., and R. Voigt. 2004. *Hydrogeologische Methoden*. Berlin: Springer verlag.

Lapham, W.W. 1989. Use of temperature profiles beneath streams to determine rates of vertical ground-water flow and vertical hydraulic conductivity. Water-Supply Paper 2337. Denver, Colorado: USGS.

Lazzari, S., A. Priarone, and E. Zanchini. 2010. Long-term performance of BHE (borehole heat exchanger) fields with negligible groundwater movement. *Energy 35*: 4966–4974.

Lee, C.K., and H.N. Lam. 2008. Computer simulation of borehole ground heat exchangers for geothermal heat pump systems. *Renew. Energ.* 33 no. 6: 1286–1296.

Lessoff, S.C., U. Schneidewind, C. Leven, P. Blum, P. Dietrich, and G. Dagan. 2010. Spatial characterization of the hydraulic conductivity using direct-push injection logging. *Water Resour. Res.* 46 no. 12: W12502, doi:10.1029/2009WR008949.

Levec, J., and R.G. Carbonell. 1985. Longitudinal and Lateral Thermal Dispersion in Packed Beds. Part II. Comparison between theory and experiment. *AIChE J.* 31 no. 4: 591–602.

Lu, X. 2009. Experimental Investigation of Thermal Dispersion in Saturated Soils with One-Dimensional Water Flow. *Soil Sci. Soc. Am. J.* 73 no. 6: 1912–1920.

Lund, J.W., D.H. Freeston, and T.L. Boyd. 2005. Direct application of geothermal energy: 2005 Worldwide review. *Geothermics* 34 no. 6: 691–727.

———. 2010. Direct Utilization of Geothermal Energy 2010 Worldwide Review. In *Proceedings World Geothermal Congress*. Bali, Indonesia, 25-29 April 2010.

Ma, R., and C. Zheng. 2010. Effects of Density and Viscosity in Modeling Heat as a Groundwater Tracer. *Ground Water* 48 no. 3: 380–389.

Man, Y., H. Yang, N. Diao, J. Liu, and Z. Fang. 2010. A new model and analytical solutions for borehole and pile ground heat exchangers. *Int. J. Heat Mass Tran.* 53 no. 13-14: 2593–2601.

Marcotte, D., and P. Pasquier. 2008. Fast fluid and ground temperature computation for geothermal ground-loop heat exchanger systems. *Geothermics* 37 no. 6: 651–665.

Marcotte, D., P. Pasquier, F. Sheriff, and M. Bernier. 2010. The importance of axial effects for borehole design of geothermal heat-pump systems. *Renew. Energ.* 35 no. 4: 763–770.

Metzger, T., S. Didierjean, and D. Maillet. 2004. Optimal experimental estimation of thermal dispersion coefficients in porous media. *Int. J. Heat Mass Tran.* 47 no. 14-16: 3341–3353.

Michopoulos, A., and N. Kyriakis. 2009. Predicting the fluid temperature at the exit of the vertical ground heat exchangers. *Appl. Energ.* 86 no. 10: 2065–2070.

Molson, J.W., E.O. Frind, and C.D. Palmer. 1992. Thermal energy storage in an unconfined aquifer: 2. Model development, validation, and application. *Water Resour. Res.* 28 no. 10: 2857–2867.

Moyne, C., S. Didierjean, H.P. Amaral Souto, and O.T. da Silveira. 2000. Thermal dispersion in porous media: one-equation model. *Int. J. Heat Mass Tran.* 43 no. 20: 3853–3867.

Mustafa Omer, A. 2008. Ground-source heat pumps systems and applications. *Renew. Sust. Energ. Rev.* 12 no. 2: 344–371.

Nam, Y., R. Ooka, and S. Hwang. 2008. Development of a numerical model to predict heat exchange rates for a ground-source heat pump system. *Energ. Buildings* 40 no. 12: 2133–2140.

Neuman, S.P. 1990. Universal Scaling of Hydraulic Conductivities and Dispersivities in Geologic Media. *Water Resour. Res.* 26 no. 8: 1749–1758.

Nield, D.A., and A. Bejan. 2006. *Convection in Porous Media*. 3d ed. New York: Springer.

Niswonger, R.G., and D.E. Prudic. 2003. Modeling heat as a tracer to estimate streambed seepage and hydraulic conductivity. In *Heat as a Tool for Studying the Movement of Ground Water Near Streams*, ed. D.A. Stonestrom and J. Constantz, 81–89. USGS Circular 1260. Reston, Virginia: USGS.

Niswonger, R.G., D.E. Prudic, G. Pohll, and J. Constantz. 2005. Incorporating seepage losses into the unsteady streamflow equations for simulating intermittent flow along mountain front streams. *Water Resour. Res.* 41 no. 6: W06006, doi:10.1029/2004WR003677.

Pannike, S., M. Kölling, B. Panteleit, J. Reichling, V. Scheps, and H.D. Schulz. 2006. Auswirkung hydrogeologischer Kenngrößen auf die Kältefahnen von Erdwärmesondenanlagen in Lockersedimenten. *Grundwasser* 11: 6–18.

Pedras, M.H.J., and M.J.S. de Lemos. 2008. Thermal dispersion in porous media as a function of the solid-fluid conductivity ratio. *Int. J. Heat Mass Tran.* 51 no. 21-22: 5359-5367.

Philippe, M., M. Bernier, and D. Marchio. 2009. Validity ranges of three analytical solutions to heat transfer in the vicinity of single boreholes. *Geothermics* 38 no. 4: 407-413.

Raymond, J., R. Therrien, L. Gosselin, and R. Lefebvre. 2011. Numerical analysis of thermal response tests with a groundwater flow and heat transfer model. *Renew. Energ.* 36 no. 1: 315–324.

Riva, M., L. Guadagnini, A. Guadagnini, T. Ptak, and E. Martac. 2006. Probabilistic study of well capture zones distribution at the Lauswiesen field site. *J. Contam. Hydrol.* 88 no. 1-2: 92–118.

Ronan, A.D., D.E. Prudic, C.E. Thodal, and J. Constantz. 1998. Field study and simulation of diurnal temperature effects on infiltration and variably saturated flow beneath an ephemeral stream. *Water Resour. Res.* 34 no. 9: 2137–2153.

Saner, D., R. Juraske, M. Kübert, P. Blum, S. Hellweg, and P. Bayer. 2010. Is it only CO_2 that matters? A life cycle perspective on shallow geothermal systems. *Renew. Sust. Energ. Rev.* 14 no. 7: 1798–1813.

Sanner, B., C. Karytsas, D. Mendrinos, and L. Rybach. 2003. Current status of ground source heat pumps and underground thermal energy storage in Europe. *Geothermics* 32: 579–588.

Sauty, J.P., A.C. Gringarten, H. Fabris, D. Thiery, A. Menjoz, and P.A. Landel. 1982a. Sensible energy storage in aquifers - 2. Field experiments and comparison with theoretical results. *Water Resour. Res.* 18 no. 1: 253–265.

Sauty, J.P., A.C. Gringarten, A. Menjoz, and P.A. Landel. 1982b. Sensible Energy Storage in Aquifers 1. Theoretical Study. *Water Resour. Res.* 18 no. 2: 245–252.

Schulze-Makuch, D. 2005. Longitudinal dispersivity data and implications for scaling behavior. *Ground Water* 43 no. 3: 443–456.

Signorelli, S., S. Bassetti, D. Pahud, and T. Kohl. 2007. Numerical evaluation of thermal response tests. *Geothermics* 36 no. 2: 141–166.

Smith, L., and D.S. Chapman. 1983. On the Thermal Effects of Groundwater Flow 1. Regional Scale Systems. *J. Geophys. Res.* 88 no. B1: 593–608.

Spitz, K., and J. Moreno. 1996. *A practical guide to groundwater and solute transport modeling*. New York: John Wiley & Sons Inc.

Stallman, R.W. 1965. Steady one-dimensional fluid flow in a semi-infinite porous medium with sinusoidal surface temperature. *J. Geophys. Res.* 70 no. 12: 2821–2827.

Stonestrom, D.A., and K.W. Blasch. 2003. Determining temperature and thermal properties for heat-based studies of surface-water ground-water interactions. In Heat as a Tool for Studying the Movement of Ground Water Near Streams, ed. D.A. Stonestrom and J. Constantz, 73–80. USGS Circular 1260. Reston, Virginia: USGS.

Su, G.W., J. Jasperse, D. Seymour, and J. Constantz. 2004. Estimation of hydraulic conductivity in an alluvial system using temperatures. *Ground Water* 42 no. 6: 890–901.

Sutton, M.G., D.W. Nutter, and R.J. Couvillion. 2003. A ground resistance for vertical borehole heat exchangers with groundwater flow. *J. Energ. Resour.-ASME* 125 no. 3: 183–189.

Suzuki, S. 1960. Percolation measurements based on heat flow through soil with special reference to Paddy fields. *J. Geophys. Res.* 65 no. 9: 2883–2885.

Taniguchi, M. 1993. Evaluation of Vertical Groundwater Fluxes and Thermal Properties of Aquifers Based on Transient Temperature-Depth Profiles. *Water Resour. Res.* 29, no. 7: 2021–2026.

van Genuchten, M.T. 1980. A Closed-form equation for predicting the hydraulic conductivity of unsaturated soils. *Soil Sci. Soc. Am. J.* 44 no. 5: 892–898.

Vandenbohede, A., A. Louwyck, and L. Lebbe. 2008. Conservative solute versus heat transport in porous media during push-pull tests. *Transp. Porous Med.* 76 no. 2: 265–287.

VDI. 2000. *Verein Deutscher Ingenieure, Blatt 1: Thermische Nutzung des Untergrundes-Grundlagen, Genehmigungen, Umweltaspekte [Part 1: Thermal use of the underground-Fundamentals, approvals, environmental aspects], VDI- 4640/1, 2000*.

———. 2001. *Verein Deutscher Ingenieure, Blatt 2: Thermische Nutzung des Untergrundes-Erdgekoppelte Wärmepumpenanlagen [Part 2: Thermal use of the underground-Ground source heat pump systems], VDI-4640/2, 2001*.

Vogt, T., P. Schneider, L. Hahn-Woernle, and O.A. Cirpka. 2010. Estimation of seepage rates in a losing stream by means of fiber-optic high-resolution vertical temperature profiling. *J. Hydrol.* 380 no. 1-2: 154–164.

Voss, C.I. 1984. SUTRA: a finite element simulation model for saturated-unsaturated, fluid-density-dependent groundwater flow energy trasnport or chemical-reactive single-species solute

transport. US Geol Surv Water Resour Invest Rep 84-4369, U.S. Geol. Surv., Reston, Virginia, 409 pp.

Wang, H., C. Qi, H. Du, and J. Gu. 2009. Thermal performance of borehole heat exchanger under groundwater flow: A case study from Baoding. *Energ. Buildings* 41 no. 12: 1368–1373.

Windqvist, G., and H. Hyden. 1976. Heat transfer in groundwater, VBB Rep. 92203543. VBB.

Woessner, W.W. 2000. Stream and Fluvial Plain Ground Water Interactions: Rescaling Hydrogeologic Thought. *Ground Water* 38 no. 3: 423–429.

Woodbury, A.D., and L. Smith. 1985. On the Thermal Effects of Three-Dimensional Groundwater Flow. *J. Geophys. Res.* 90 no. B1: 759–767.

Xu, M., and Y. Eckstein. 1995. Use of Weighted Least-Squares Method in Evaluation of the Relationship Between Dispersivity and Field Scale. *Ground Water* 33 no. 6: 905–908.

Yang, W., M. Shi, G. Liu, and Z. Chen. 2009. A two-region simulation model of vertical U-tube ground heat exchanger and its experimental verification. *Appl. Energ.* 86 no. 10: 2005–2012.

Yavuzturk, C. 1999. Modeling of Vertical Ground Loop Heat Exchangers for Ground Source Heat Pump Systems. PhD Thesis, Oklahoma State University, Stillwater, Oklahoma, U.S.A.

Yuan, Z.-G., W.H. Somerton, and K.S. Udell. 1991. Thermal dispersion in thick-walled tubes as a model of porous media. *Int. J. Heat Mass Tran.* 34 no. 11: 2715–2726.

Zeng, H.Y., N.R. Diao, and Z.H. Fang. 2002. A finite line-source model for boreholes in geothermal heat exchangers. *Heat Transfer–Asian Research* 31 no. 7: 558–567.

Zubair, S., and M. Chaudhry. 1996. Temperature solutions due to time-dependent moving-line-heat sources. *Heat Mass Transfer* 31 no. 3: 185–189.